

Formation Path Following Control of Underactuated AUVs – With Proofs

Josef Matouš Kristin Y. Pettersen Claudio Paliotta

Abstract—This paper proposes a novel method for formation path following of multiple underactuated autonomous underwater vehicles. The method combines line-of-sight guidance with null-space-based behavioral control, allowing the vehicles to follow curved paths while maintaining the desired formation. We investigate the dynamics of the path-following error using cascaded systems theory, and show that the closed-loop system is uniformly semi-globally exponentially stable. We validate the theoretical results through numerical simulations.

I. INTRODUCTION

Autonomous underwater vehicles (AUVs) are being increasingly used in a number of applications such as transportation, seafloor mapping, and the ocean energy industry. Some complex tasks need to be performed by a group of cooperating AUVs. Consequently, there is a need for control algorithms that can guide a formation of AUVs along a given path while avoiding collisions with each other.

A comprehensive overview of various formation path-following methods is presented in [1]. Most of these methods are based on two concepts: coordinated path-following [2], [3], and leader-follower [4], [5]. In the *coordinated path-following* approach, each vehicle follows a predefined path separately. Formation is then achieved by coordinating the motion of the vehicles along these paths. In this approach, the formation-keeping error (*i.e.*, the difference between the actual and desired relative position of the vehicles) may initially grow as the vehicles converge to their predefined paths. In the *leader-follower* approach, one leading vehicle follows the given path while the followers adjust their speed and position to obtain the desired formation shape. This approach tends to suffer from the lack of formation feedback due to unidirectional communication (*i.e.*, the leader does not adjust its velocity based on the followers).

The null-space-based behavioral (NSB) algorithm has also been proposed to solve the formation path-following problem [6]–[9]. The NSB algorithm is a centralized control method that allows to combine several hierarchic tasks. In the NSB framework, it is possible to design the path-following, formation-keeping, and collision avoidance tasks independently. By combining these tasks, the vehicles exhibit the desired behavior.

This paper aims to extend the results of [9], where an NSB algorithm is used to guide two surface vessels moving

in the horizontal plane. Specifically, we propose an algorithm that works with an arbitrary number of AUVs with five degrees of freedom (DOFs) moving in 3D. Similarly to [9], we solve the path-following task using line-of-sight (LOS) guidance. Using the cascaded systems theory results of [10], we prove that the closed-loop system consisting of a 3D LOS guidance law, combined with surge, pitch, and yaw autopilots based on [11], is uniformly semi-globally exponentially stable (USGES) and uniformly globally asymptotically stable (UGAS). The theoretical results are verified through numerical simulations.

The remainder of the paper is organized as follows. Section II introduces the model of the AUVs. In Section III, we define the formation path-following problem. In Section IV, we describe the control system. The stability of the control system is proven in Section V. Section VI contains the results of a numerical simulation. Finally, Section VII contains some concluding remarks.

II. MODEL

In this section, we present the model of the AUV. We start by introducing the model in a matrix-vector form. Then, we write out the ordinary differential equations (ODEs) for the individual state variables.

A. Vehicle Model in Vector-Matrix Form

The pose ($\boldsymbol{\eta}$) and velocities ($\boldsymbol{\nu}$) of an AUV with 5DOFs are defined as

$$\boldsymbol{\eta} = [x, y, z, \theta, \psi]^T, \quad \boldsymbol{\nu} = [u, v, w, q, r]^T, \quad (1)$$

where x, y, z are the coordinates of the vehicle in North-East-Down (NED) coordinate frame, and θ and ψ are the pitch and yaw angles, respectively. The velocities u, v, w are the linear surge, sway and heave velocities in a given body-fixed frame, and q and r are the pitch and yaw rate, respectively. The roll dynamics are disregarded as the roll motion is assumed to be small and self-stabilizing by the vehicle design.

Let $\mathbf{V}_c = [V_x, V_y, V_z]^T$ be the velocities of an unknown, constant and irrotational ocean current, given in the inertial NED frame. Let $\mathbf{J}(\boldsymbol{\eta})$ be the transformation matrix from the body-fixed to the inertial frame. $\mathbf{J}(\boldsymbol{\eta})$ is given by

$$\mathbf{J}(\boldsymbol{\eta}) = \begin{bmatrix} \mathbf{R}(\theta, \psi) & \mathbf{O}_{3 \times 2} \\ \mathbf{O}_{2 \times 3} & \mathbf{T}(\theta) \end{bmatrix}, \quad (2)$$

where $\mathbf{R}(\theta, \psi)$ is the rotation matrix from the body-fixed to the inertial coordinate frames, $\mathbf{O}_{n \times m}$ is an $n \times m$ matrix of zeros, and $\mathbf{T}(\theta) = \text{diag}(1, 1/\cos\theta)$, which is well-defined if the pitch angle $|\theta| < \pi/2$. Note that the mechanical design of

Josef Matouš and Kristin Y. Pettersen are with the Centre for Autonomous Marine Operations and Systems, Department of Engineering Cybernetics, Norwegian University of Science and Technology (NTNU), Trondheim, Norway. {josef.matous, kristin.y.pettersen}@ntnu.no. Claudio Paliotta is with SINTEF Digital, Trondheim, Norway. claudio.paliotta@sintef.no

torpedo-shaped rudder-controlled AUVs generally does not allow for pitch angles $|\theta| = \pi/2$.

The velocities of the ocean current expressed in the body-fixed coordinate frame, $\boldsymbol{\nu}_c$, are thus

$$\boldsymbol{\nu}_c = \left[\left(\mathbf{R}(\theta, \psi)^T \mathbf{V}_c \right)^T, 0, 0 \right]^T. \quad (3)$$

We will denote the relative velocities of the vehicle as $\boldsymbol{\nu}_r = \boldsymbol{\nu} - \boldsymbol{\nu}_c$. We will also denote the relative surge, sway and heave velocities as u_r, v_r and w_r , respectively.

Let $\mathbf{f} = [T_u, \delta_e, \delta_r]$ be the vector of control inputs, where T_u is the surge thrust generated by the propeller, and δ_e and δ_r are the deflection angles of the elevator and rudder, respectively. Furthermore, let \mathbf{M} be the mass and inertia matrix, including added mass effects, $\mathbf{C}(\boldsymbol{\nu}_r)$ the Coriolis centripetal matrix, also including added mass effects, and $\mathbf{D}(\boldsymbol{\nu}_r)$ the hydrodynamic damping matrix. The dynamics of the vehicle in a matrix-vector form are then [12]

$$\dot{\boldsymbol{\eta}} = \mathbf{J}(\boldsymbol{\eta}) \boldsymbol{\nu}, \quad (4)$$

$$\mathbf{M}\dot{\boldsymbol{\nu}}_r + \mathbf{C}(\boldsymbol{\nu}_r) \boldsymbol{\nu}_r + \mathbf{D}(\boldsymbol{\nu}_r) \boldsymbol{\nu}_r + \mathbf{g}(\boldsymbol{\eta}) = \mathbf{B}\mathbf{f}, \quad (5)$$

where $\mathbf{g}(\boldsymbol{\eta})$ is the gravity and buoyancy vector, and \mathbf{B} is the actuator configuration matrix that maps the control inputs to forces and torques.

B. Vehicle Model in Component Form

First, let us present the necessary assumptions for deriving the ODEs for individual state variables.

Assumption 1: The vehicle is slender, torpedo-shaped with port-starboard symmetry.

Assumption 2: The hydrodynamic damping is linear.

Assumption 3: The vehicle is neutrally buoyant with the center of gravity (CG) and the center of buoyancy (CB) located along the same vertical axis.

Remark: Assumptions 1 and 3 are valid from the mechanical design of commercial survey AUVs. Assumption 2 is valid for low-speed missions. Also for higher-speed missions, this assumption is often made when designing the controller, as the higher-order damping coefficients are poorly known, and the forces are dissipative. Attempting to cancel the higher-order damping can thus introduce destabilizing control efforts.

Under these assumptions, the \mathbf{M} and \mathbf{B} matrices have the following form

$$\mathbf{M} = \begin{bmatrix} m_{11} & 0 & 0 & 0 & 0 \\ 0 & m_{22} & 0 & 0 & m_{25} \\ 0 & 0 & m_{33} & m_{34} & 0 \\ 0 & 0 & m_{34} & m_{44} & 0 \\ 0 & m_{25} & 0 & 0 & m_{55} \end{bmatrix}, \quad \mathbf{B} = \begin{bmatrix} b_{11} & 0 & 0 \\ 0 & 0 & b_{23} \\ 0 & b_{32} & 0 \\ 0 & b_{42} & 0 \\ 0 & 0 & b_{53} \end{bmatrix} \quad (6)$$

the corresponding Coriolis matrix is

$$\mathbf{C}(\boldsymbol{\nu}_r) = \begin{bmatrix} 0 & 0 & 0 & c_1 & -c_2 \\ 0 & 0 & 0 & 0 & c_3 \\ 0 & 0 & 0 & -c_3 & 0 \\ -c_1 & 0 & c_3 & 0 & 0 \\ c_2 & -c_3 & 0 & 0 & 0 \end{bmatrix}, \quad (7)$$

where $c_1 = m_{34} q + m_{33} w_r$, $c_2 = m_{25} r + m_{22} v_r$, and

$c_3 = m_{11} u_r$. The hydrodynamic damping matrix is

$$\mathbf{D}(\boldsymbol{\nu}_r) \approx \mathbf{D} = \begin{bmatrix} d_{11} & 0 & 0 & 0 & 0 \\ 0 & d_{22} & 0 & 0 & d_{25} \\ 0 & 0 & d_{33} & d_{34} & 0 \\ 0 & 0 & d_{43} & d_{44} & 0 \\ 0 & d_{52} & 0 & 0 & d_{55} \end{bmatrix}, \quad (8)$$

and the gravity vector has the following form

$$\mathbf{g}(\boldsymbol{\eta}) = [0, 0, 0, m g z_g \sin(\theta)]^T, \quad (9)$$

where m is the weight of the vessel, g is the gravity acceleration, and z_g is the vertical distance between the CG and CB [12].

Furthermore, we assume that the actuators produce no sway and heave acceleration. In other words, for every \mathbf{f} there exist f_u, t_q and t_r such that

$$\mathbf{M}^{-1} \mathbf{B}\mathbf{f} = [f_u, 0, 0, t_q, t_r]^T. \quad (10)$$

In [13], it is shown that if a vehicle satisfies Assumptions 1–3, the origin of the body-fixed coordinate frame can always be chosen such that (10) holds.

Under these assumptions, the model can expressed in the following form

$$\dot{x} = u \cos(\psi) \cos(\theta) - v \sin(\psi) + w \cos(\psi) \sin(\theta), \quad (11a)$$

$$\dot{y} = u \cos(\theta) \sin(\psi) + v \cos(\psi) + w \sin(\psi) \sin(\theta), \quad (11b)$$

$$\dot{z} = -u \sin(\theta) + w \cos(\theta), \quad (11c)$$

$$\dot{\theta} = q, \quad (11d)$$

$$\dot{\psi} = \frac{1}{\cos(\theta)} r, \quad (11e)$$

$$\dot{u} = f_u + F_u(u, v, w, q, r) + \phi_u(u, v, w, q, r, \theta, \psi)^T \mathbf{V}_c, \quad (11f)$$

$$\dot{v} = X_v(u, u_c) r + Y_v(u, u_c) v_r, \quad (11g)$$

$$\dot{w} = X_w(u, u_c) q + Y_w(u, u_c) w_r + G(\theta), \quad (11h)$$

$$\dot{q} = t_q + F_q(u, w, q, \theta) + \phi_q(u, w, q, \theta, \psi)^T \boldsymbol{\vartheta}(\mathbf{V}_c), \quad (11i)$$

$$\dot{r} = t_r + F_r(u, v, r) + \phi_r(u, v, r, \theta, \psi)^T \boldsymbol{\vartheta}(\mathbf{V}_c), \quad (11j)$$

where $\boldsymbol{\vartheta}(\mathbf{V}_c) = [V_x, V_y, V_z, V_x^2, V_y^2, V_z^2, V_x V_y, V_x V_z, V_y V_z]^T$, and the expressions for $F_i(\cdot)$, $\phi_i(\cdot)$, $i \in \{u, q, r\}$, $X_v(\cdot)$, $Y_v(\cdot)$, $X_w(\cdot)$, $Y_w(\cdot)$, and $G(\cdot)$ are given in Appendix I.

III. CONTROL OBJECTIVES

The goal is to control n AUVs so that they move in a prescribed formation while avoiding collisions, and their barycenter follows a given path.

The prescribed path in the inertial coordinate frame is given by a smooth function $\mathbf{p}_p : \mathbb{R} \rightarrow \mathbb{R}^3$. We assume that the path function is \mathcal{C}^2 and regular, *i.e.*, the function is continuous up to its second derivative and its first derivative with respect to the path parameter satisfies

$$\left\| \frac{\partial \mathbf{p}_p(\xi)}{\partial \xi} \right\| \neq 0. \quad (12)$$

Therefore, for every point $\mathbf{p}_p(\xi)$ on the path, there exist path-tangential angles, $\theta_p(\xi)$ and $\psi_p(\xi)$, and a corresponding path-tangential coordinate frame (x^p, y^p, z^p) (see Figure 1).

The path-following error \mathbf{p}_b^p is given by the position of the barycenter expressed in the path-tangential coordinate frame

$$\mathbf{p}_b^p = \mathbf{R}(\theta_p(\xi), \psi_p(\xi))^T (\mathbf{p}_b - \mathbf{p}_p(\xi)), \quad (13)$$

where

$$\mathbf{p}_b = \frac{1}{n} \sum_{i=1}^n \mathbf{p}_i, \quad \mathbf{p}_i = [x_i, y_i, z_i]^T, \quad (14)$$

where (x_i, y_i, z_i) is the position of the i^{th} vehicle. The goal of path following is to control the vehicles so that $\mathbf{p}_b^p \equiv \mathbf{0}_3$, where $\mathbf{0}_3$ is a 3-element vector of zeros.

To define the formation-keeping problem, we first define the formation-centered coordinate frame. This coordinate frame is created by translating the path-tangential frame into the barycenter (see Figure 2). Let $\mathbf{p}_{f,1}^f, \dots, \mathbf{p}_{f,n}^f$ be the position vectors that represent the desired formation. These vectors should be chosen such that their mean is equal to the barycenter. Since the barycenter is equivalent to the origin of the formation-centered frame, the vectors must thus satisfy

$$\sum_{i=1}^n \mathbf{p}_{f,i}^f = \mathbf{0}_3. \quad (15)$$

The position of vehicle i in the formation-centered frame is

$$\mathbf{p}_i^f = \mathbf{R}^T(\theta_p(\xi), \psi_p(\xi)) (\mathbf{p}_i - \mathbf{p}_b). \quad (16)$$

The goal of formation keeping is to have $\mathbf{p}_i^f \equiv \mathbf{p}_{f,i}^f$. This problem can also be expressed in the inertial coordinate frame as

$$\mathbf{p}_i \equiv \mathbf{R}(\theta_p(\xi), \psi_p(\xi)) \mathbf{p}_{f,i}^f + \mathbf{p}_b, \quad i \in \{1, \dots, n\}. \quad (17)$$

IV. CONTROL SYSTEM

To solve the formation path following problem, we propose a method that combines collision avoidance (COLAV), formation keeping, and LOS path following in a hierarchical manner using an NSB algorithm. Since the NSB algorithm outputs velocity references, we also need a low-level attitude control system to track these references.

In this section, we first present the attitude control system. Then, in Section IV-B, we present the NSB algorithm and the associated COLAV and formation keeping tasks. In Section IV-C, we present the LOS guidance law for path following. Finally, in Section IV-D, we demonstrate how to use the path variable update law to cancel unwanted terms in the path following error dynamics.

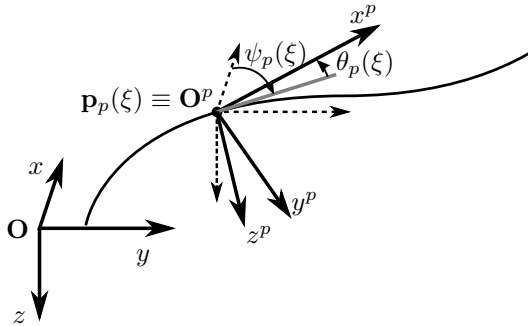


Fig. 1. Definition of the path angles and path-tangential coordinate frame. \mathbf{O} denotes the origin of the inertial coordinate frame, \mathbf{O}^p denotes the origin of the path-tangential frame, the grey line represents the projection of the path-tangential vector into the xy -plane.

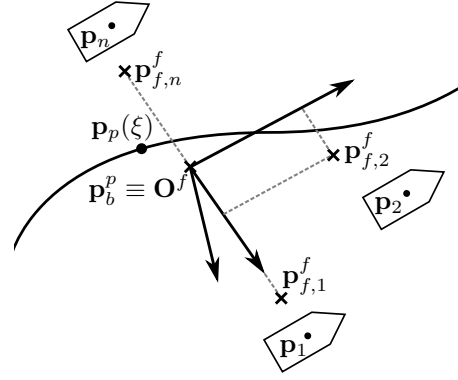


Fig. 2. Definition of the formation. \mathbf{O}^f denotes the origin of the formation-centered coordinate frame.

A. Attitude Control System

This system controls the surge velocity, pitch, and yaw via the corresponding accelerations. The system is based on the autopilots in [11], but extended to 5DOFs.

Let u_d be the desired surge velocity and \dot{u}_d its derivative. Let $\hat{\mathbf{V}}_c$ be the estimate of the ocean current. Furthermore, let us define $\tilde{u} = u - u_d$ and $\tilde{\mathbf{V}}_c = \hat{\mathbf{V}}_c - \mathbf{V}_c$. The surge controller consists of an output-linearizing sliding-mode P-controller and an ocean current observer

$$f_u = \dot{u}_d - F_u(\cdot) - \phi_u(\cdot)^T \hat{\mathbf{V}}_c - k_u \tilde{u} - k_c \text{sign}(\tilde{u}), \quad (18)$$

$$\dot{\hat{\mathbf{V}}}_c = c_u \phi_u(\cdot) \tilde{u}, \quad (19)$$

where k_u , k_c and c_u are positive gains.

Let θ_d be the desired pitch angle and $\dot{\theta}_d, \ddot{\theta}_d$ its derivatives. Let $\hat{\boldsymbol{\vartheta}}_q$ be the estimate of $\boldsymbol{\vartheta}(\mathbf{V}_c)$. Furthermore, let us define $\tilde{\theta} = \theta - \theta_d$, $\tilde{q} = q - \dot{\theta}_d$ and $\tilde{\boldsymbol{\vartheta}}_q = \hat{\boldsymbol{\vartheta}}_q - \boldsymbol{\vartheta}(\mathbf{V}_c)$. Inspired by [14], we introduce the following transformation

$$s_q = \tilde{q} + \lambda_q \tilde{\theta}, \quad (20)$$

where λ_q is a positive constant. The pitch controller consists of an output-linearizing sliding-mode PD-controller and an ocean current observer

$$t_q = \ddot{\theta}_d - F_q(\cdot) - \phi_q(\cdot)^T \hat{\boldsymbol{\vartheta}}_q - \lambda_q \tilde{q} - k_\theta \tilde{\theta} - k_q s_q - k_d \text{sign}(s_q), \quad (21)$$

$$\dot{\hat{\boldsymbol{\vartheta}}}_q = c_q \phi_q(\cdot) s_q, \quad (22)$$

where k_θ , k_q , k_d and c_q are positive gains.

Let ψ_d be the desired yaw angle and $\dot{\psi}_d, \ddot{\psi}_d$ its derivatives. Let $\hat{\boldsymbol{\vartheta}}_r$ be the estimate of $\boldsymbol{\vartheta}(\mathbf{V}_c)$. Furthermore, let us define $\tilde{\psi} = \psi - \psi_d$ and $\tilde{\boldsymbol{\vartheta}}_r = \hat{\boldsymbol{\vartheta}}_r - \boldsymbol{\vartheta}(\mathbf{V}_c)$. Similarly to the pitch controller, we introduce the following transformation

$$s_r = \dot{\tilde{\psi}} + \lambda_r \tilde{\psi} = \frac{r}{\cos \theta} - \dot{\psi}_d + \lambda_r \tilde{\psi}, \quad (23)$$

where λ_r is a positive constant. The yaw controller is analogous to the pitch controller introduced in the previous section

$$t_r = -F_r(\cdot) - \phi_r(\cdot)^T \hat{\boldsymbol{\vartheta}}_r - r \tan(\theta) \dot{\theta} + \cos(\theta) \left(\ddot{\psi}_d - \lambda_r \dot{\tilde{\psi}} - k_\psi \tilde{\psi} - k_r s_r - k_d \text{sign}(s_r) \right), \quad (24)$$

$$\dot{\hat{\boldsymbol{\vartheta}}}_r = c_r \phi_r(\cdot) s_r, \quad (25)$$

where k_ψ , k_r , k_d and c_r are positive gains.

B. NSB Tasks

Let us denote the variables associated with the COLAV, formation keeping, and path following tasks by lower indices 1, 2, and 3, respectively. Each task produces a vector of desired velocities, $\mathbf{v}_{d,i} \in \mathbb{R}^{3n}$, $i \in \{1, 2, 3\}$.

For the COLAV and formation keeping tasks, the desired velocities are obtained using task variables, $\boldsymbol{\sigma}_1$ and $\boldsymbol{\sigma}_2$, and their desired values, $\boldsymbol{\sigma}_{d,1}$ and $\boldsymbol{\sigma}_{d,2}$.

First, let us consider the COLAV task. Let d_{COLAV} be the *activation distance*, i.e., the distance at which the vehicles need to start performing the evasive maneuvers. The task variable is then given by a vector of relative distances between the vehicles smaller than d_{COLAV} , i.e.,

$$\boldsymbol{\sigma}_1 = [\|\mathbf{p}_i - \mathbf{p}_j\|]^T, \quad \forall i, j \in \{1, \dots, n\}, j > i, \quad (26)$$

$$\|\mathbf{p}_i - \mathbf{p}_j\| < d_{\text{COLAV}}.$$

The desired values of the task are

$$\boldsymbol{\sigma}_{1,d} = d_{\text{COLAV}} \mathbf{1}, \quad (27)$$

where $\mathbf{1}$ is a vector of ones. Note that this task does not guarantee robust collision avoidance. During the transients, the relative distance may become smaller than d_{COLAV} . Therefore, to ensure collision avoidance, d_{COLAV} should be chosen as $d_{\text{min}} + d_{\text{sec}}$, where d_{min} is the minimum safe distance between the vehicles, and d_{sec} is an additional security distance.

Now, let us consider the formation keeping task. The task variable is defined as

$$\boldsymbol{\sigma}_2 = [\boldsymbol{\sigma}_{2,1}^T, \dots, \boldsymbol{\sigma}_{2,n-1}^T]^T, \quad \boldsymbol{\sigma}_{2,i} = \mathbf{p}_i - \mathbf{p}_b, \quad (28)$$

and its desired values are

$$\boldsymbol{\sigma}_{d,2} = \begin{bmatrix} \mathbf{R}(\theta_p(\xi), \psi_p(\xi)) \mathbf{p}_{f,1}^p \\ \vdots \\ \mathbf{R}(\theta_p(\xi), \psi_p(\xi)) \mathbf{p}_{f,n-1}^p \end{bmatrix}. \quad (29)$$

The desired velocities of the COLAV and formation keeping tasks are obtained using the closed-loop inverse kinematics (CLIK) equation [6]

$$\mathbf{v}_{d,i} = \mathbf{J}_i^\dagger (\dot{\boldsymbol{\sigma}}_{d,i} - \boldsymbol{\Lambda}_i \tilde{\boldsymbol{\sigma}}_i), \quad i \in \{1, 2\}, \quad (30)$$

where $\tilde{\boldsymbol{\sigma}}_i = \boldsymbol{\sigma}_i - \boldsymbol{\sigma}_{d,i}$ is the error, \mathbf{J}^\dagger is the Moore-Penrose pseudoinverse, $\boldsymbol{\Lambda}_i$ is a positive definite gain matrix, and \mathbf{J}_i is the task Jacobian given by

$$\mathbf{J}_i = \frac{\partial \boldsymbol{\sigma}_i}{\partial \mathbf{p}}, \quad \mathbf{p} = [\mathbf{p}_1^T, \dots, \mathbf{p}_n^T]^T. \quad (31)$$

The desired velocity of the path-following task is obtained using LOS guidance that is explained in the next section. These velocities are then combined using the NSB algorithm

$$\mathbf{v}_{\text{NSB}} = \mathbf{v}_{d,1} + (\mathbf{I} - \mathbf{J}_1^\dagger \mathbf{J}_1) (\mathbf{v}_{d,2} + (\mathbf{I} - \mathbf{J}_2^\dagger \mathbf{J}_2) \mathbf{v}_{d,3}), \quad (32)$$

if there are active COLAV tasks, and

$$\mathbf{v}_{\text{NSB}} = \mathbf{v}_{d,2} + (\mathbf{I} - \mathbf{J}_2^\dagger \mathbf{J}_2) \mathbf{v}_{d,3}, \quad (33)$$

if there are none (\mathbf{I} is an identity matrix). The NSB velocities

must be decomposed into surge, pitch, and yaw references that can be tracked by the attitude control system presented in Section IV-A. Similarly to [6], we propose a method with angle of attack and sideslip compensation

$$u_{d,i} = U_{\text{NSB},i} \frac{1 + \cos(\gamma_{\text{NSB},i} - \gamma_i) \cos(\chi_{\text{NSB},i} - \chi_i)}{2}, \quad (34)$$

$$\theta_{d,i} = \gamma_{\text{NSB},i} + \alpha_{d,i}, \quad \alpha_{d,i} = \arctan\left(\frac{w_i}{u_{d,i}}\right), \quad (35)$$

$$\psi_{d,i} = \chi_{\text{NSB},i} - \beta_{d,i}, \quad \beta_{d,i} = \arcsin\left(\frac{v_i}{\sqrt{u_{d,i}^2 + v_i^2 + w_i^2}}\right), \quad (36)$$

where v_i and w_i are the sway and heave velocities, and γ_i and χ_i are the flight-path and course angles of the i^{th} vehicle, respectively, and $U_{\text{NSB},i}$, $\gamma_{\text{NSB},i}$ and $\chi_{\text{NSB},i}$ are given by

$$U_{\text{NSB},i} = \|\mathbf{v}_{\text{NSB},i}\|, \quad \mathbf{v}_{\text{NSB},i} = \begin{bmatrix} \dot{x}_{\text{NSB},i} \\ \dot{y}_{\text{NSB},i} \\ \dot{z}_{\text{NSB},i} \end{bmatrix}, \quad (37a)$$

$$\gamma_{\text{NSB},i} = -\arcsin\left(\frac{\dot{y}_{\text{NSB},i}}{U_{\text{NSB},i}}\right), \quad (37b)$$

$$\chi_{\text{NSB},i} = \arctan_2(\dot{y}_{\text{NSB},i}, \dot{x}_{\text{NSB},i}), \quad (37c)$$

where $\arctan_2(y, x)$ is the four-quadrant inverse tan.

C. Line-of-Sight Guidance

The desired flight-path angle and course of the path-following task are given by the following LOS law

$$\gamma_{\text{LOS}} = \theta_p(\xi) + \arctan\left(\frac{z_b^p}{\Delta(\mathbf{p}_b^p)}\right), \quad (38)$$

$$\chi_{\text{LOS}} = \psi_p(\xi) - \arctan\left(\frac{y_b^p}{\Delta(\mathbf{p}_b^p)}\right), \quad (39)$$

where $\mathbf{p}_b^p = [x_b^p, y_b^p, z_b^p]^T$, and $\Delta(\mathbf{p}_b^p)$ is the lookahead distance. Inspired by [15], we choose the lookahead distance as

$$\Delta(\mathbf{p}_b^p) = \sqrt{\Delta_0^2 + (x_b^p)^2 + (y_b^p)^2 + (z_b^p)^2}, \quad (40)$$

where $\Delta_0 > 0$ is a constant.

The desired velocity of the path-following task is then given by

$$\mathbf{v}_{d,3} = \mathbf{1}_n \otimes \mathbf{v}_{\text{LOS}}, \quad (41)$$

where $\cdot \otimes \cdot$ is the Kronecker tensor product, and

$$\mathbf{v}_{\text{LOS}} = \begin{bmatrix} \cos(\chi_{\text{LOS}}) \cos(\gamma_{\text{LOS}}) \\ \cos(\gamma_{\text{LOS}}) \sin(\chi_{\text{LOS}}) \\ -\sin(\gamma_{\text{LOS}}) \end{bmatrix} U_{\text{LOS}}, \quad (42)$$

where U_{LOS} is the desired path-following speed.

D. Path Parametrization

Inspired by [15], we use the update law of the path variable ξ to get desirable behavior of the along-track error (x_b^p).

Note that the kinematics of the i^{th} vehicle can be alternatively expressed using the total speed (U_i) and the flight-path (γ_i) and course (χ_i) angles of the vehicle as

$$\dot{\mathbf{p}}_i = [\cos(\chi_i) \cos(\gamma_i), \cos(\gamma_i) \sin(\chi_i), -\sin(\gamma_i)]^T U_i. \quad (43)$$

Now, let us investigate the kinematics of the barycenter. Differentiating (13) with respect to time and substituting (43)

yields the following equations

$$\dot{x}_b^p = \frac{1}{n} \sum_{i=1}^n U_i \Omega_x(\gamma_i, \theta_p, \chi_i, \psi_p) - \left\| \frac{\partial \mathbf{p}_p(\xi)}{\partial \xi} \right\| \dot{\xi} + \omega_z y_b^p - \omega_y z_b^p, \quad (44a)$$

$$\dot{y}_b^p = \frac{1}{n} \sum_{i=1}^n U_i \Omega_y(\gamma_i, \theta_p, \chi_i, \psi_p) + \omega_x z_b^p - \omega_z x_b^p, \quad (44b)$$

$$\dot{z}_b^p = \frac{1}{n} \sum_{i=1}^n U_i \Omega_z(\gamma_i, \theta_p, \chi_i, \psi_p) + \omega_y x_b^p - \omega_x y_b^p, \quad (44c)$$

where

$$\Omega_x(\cdot) = \sin(\theta_p) \sin(\gamma_i) + \cos(\theta_p) \cos(\gamma_i) \cos(\psi_p - \chi_i), \quad (45a)$$

$$\Omega_y(\cdot) = -\cos(\gamma_i) \sin(\psi_p - \chi_i), \quad (45b)$$

$$\Omega_z(\cdot) = -\cos(\theta_p) \sin(\gamma_i) + \cos(\gamma_i) \sin(\theta_p) \cos(\psi_p - \chi_i) \quad (45c)$$

$$\omega_x = -\iota \dot{\xi} \sin(\theta_p), \quad \omega_y = \kappa \dot{\xi}, \quad \omega_z = \iota \dot{\xi} \cos(\theta_p), \quad (45d)$$

$$\kappa(\xi) = \frac{\partial \theta_p(\xi)}{\partial \xi}, \quad \iota(\xi) = \frac{\partial \psi_p(\xi)}{\partial \xi}. \quad (45e)$$

To stabilize the along-track error dynamics, we choose the following path variable update

$$\dot{\xi} = \left\| \frac{\partial \mathbf{p}_p(\xi)}{\partial \xi} \right\|^{-1} \left(\frac{1}{n} \sum_{i=1}^n U_i \Omega_x(\gamma_i, \theta_p, \chi_i, \psi_p) + k_\xi \frac{x_b^p}{\sqrt{1 + (x_b^p)^2}} \right), \quad (46)$$

where $k_\xi > 0$ is a constant.

V. CLOSED-LOOP ANALYSIS

In this section, we investigate the closed-loop stability of the path following task. We define two error states, $\tilde{\mathbf{X}}_1$ and $\tilde{\mathbf{X}}_2$, as

$$\tilde{\mathbf{X}}_1 = [x_b^p, y_b^p, z_b^p]^T, \quad \tilde{\mathbf{X}}_2 = [\tilde{\mathbf{X}}_{2,1}^T, \dots, \tilde{\mathbf{X}}_{2,n}^T]^T, \quad (47)$$

$$\tilde{\mathbf{X}}_{2,i} = [\tilde{u}_i, s_{q,i}, \tilde{\theta}_i, s_{r,i}, \tilde{\psi}_i]^T, \quad (48)$$

Now, we can take the barycenter kinematics from (44) and express it in terms of $\tilde{\mathbf{X}}_1$ and $\tilde{\mathbf{X}}_2$ as

$$\dot{x}_b^p = -k_\xi \frac{x_b^p}{\sqrt{1 + (x_b^p)^2}} + \omega_z y_b^p - \omega_y z_b^p, \quad (49a)$$

$$\dot{y}_b^p = -\frac{1}{n} \sum_{i=1}^n U_{d,i} \frac{\cos(\gamma_{\text{LOS}}) y_b^p}{\sqrt{\Delta(\mathbf{p}_b^p)^2 + (y_b^p)^2}} + \omega_x z_b^p - \omega_z x_b^p + G_y(\tilde{u}_1, \dots, \tilde{u}_n, \tilde{\psi}_1, \dots, \tilde{\psi}_n, \gamma_1, \dots, \gamma_n, u_{d,1}, \dots, u_{d,n}, v_1, \dots, v_n, w_1, \dots, w_n, \mathbf{p}_b^p, \psi_p), \quad (49b)$$

$$\dot{z}_b^p = \frac{1}{n} \sum_{i=1}^n U_{d,i} \frac{z_b^p}{\sqrt{\Delta(\mathbf{p}_b^p)^2 + (z_b^p)^2}} + \omega_y x_b^p - \omega_x y_b^p + G_z(\tilde{u}_1, \dots, \tilde{u}_n, \tilde{\theta}_1, \dots, \tilde{\theta}_n, \gamma_1, \dots, \gamma_n, \chi_1, \dots, \chi_n, u_{d,1}, \dots, u_{d,n}, v_1, \dots, v_n, w_1, \dots, w_n, \mathbf{p}_b^p, \psi_p, \theta_p). \quad (49c)$$

The equations for $G_y(\cdot)$ and $G_z(\cdot)$ are given in Appendix II-A. Substituting the attitude control system (18)–(25) into vehicle dynamics (11) yields the following closed-loop behavior of $\tilde{\mathbf{X}}_2$

$$\dot{\tilde{u}}_i = -k_u \tilde{u}_i - k_c \text{sign}(\tilde{u}_i) - \phi_u(\cdot)^T \tilde{\mathbf{V}}_{c,i}, \quad (50a)$$

$$\dot{s}_{q,i} = -k_\theta \tilde{\theta}_i - k_q s_{q,i} - k_d \text{sign}(s_{q,i}) - \phi_q(\cdot)^T \tilde{\boldsymbol{\theta}}_{q,i}, \quad (50b)$$

$$\dot{\tilde{\theta}}_i = s_{q,i} - \lambda_q \tilde{\theta}_i, \quad (50c)$$

$$\dot{s}_{r,i} = -k_\theta \tilde{\theta}_i - k_r s_{r,i} - k_d \text{sign}(s_{r,i}) - \phi_r(\cdot)^T \tilde{\boldsymbol{\theta}}_{r,i}, \quad (50d)$$

$$\dot{\tilde{\psi}}_i = s_{r,i} - \lambda_r \tilde{\psi}_i, \quad (50e)$$

the ocean current estimate errors

$$\dot{\tilde{\mathbf{V}}}_{c,i} = c_u \phi_u(\cdot) \tilde{u}_i, \quad (51a)$$

$$\dot{\tilde{\boldsymbol{\theta}}}_{q,i} = c_q \phi_q(\cdot) s_{q,i}, \quad (51b)$$

$$\dot{\tilde{\boldsymbol{\theta}}}_{r,i} = c_r \phi_r(\cdot) s_{r,i}, \quad (51c)$$

and the underactuated sway and heave dynamics

$$\dot{v}_i = X_v(u_i, u_c) r_i + Y_v(u_i, u_c) (v_i - v_c), \quad (52)$$

$$\dot{w}_i = X_w(u_i, u_c) q_i + Y_w(u_i, u_c) (w_i - w_c) + G(\theta_i). \quad (53)$$

To prove the stability of the closed-loop system, we need the results of the three following lemmas. The lemmas follow the same structure as the 2D case for two ASVs in [9], and are extended to handle an arbitrary number of AUVs moving in 3D.

Lemma 1: The trajectories of the closed-loop system (49)–(53) are forward complete.

Proof: The proof is given in Appendix II-C. ■

Lemma 2: The underactuated sway and heave dynamics are bounded near the manifold $[\tilde{\mathbf{X}}_1^T, \tilde{\mathbf{X}}_2^T] = \mathbf{0}^T$ if $Y_v(u, u_c) < 0$, $Y_w(u, u_c) < 0$ and the curvature of the path satisfies

$$|\kappa(\xi)| < \frac{n}{2} \left| \frac{Y_w(u, u_c)}{X_w(u, u_c)} \right|, \quad |\iota(\xi)| < \frac{n}{2} \left| \frac{Y_v(u, u_c)}{X_v(u, u_c)} \right|, \quad (54)$$

for all $u > 0$ and $u_c \in [-\|\mathbf{V}_c\|, \|\mathbf{V}_c\|]$.

Proof: The proof is given in Appendix II-D. ■

Lemma 3: The underactuated sway and heave dynamics are bounded near the manifold $\tilde{\mathbf{X}}_2 = \mathbf{0}$, independently of $\tilde{\mathbf{X}}_1$ if the assumptions in Lemma 2 are satisfied and the constant term Δ_0 in the lookahead distance (40) is chosen so that

$$\Delta_0 > \max \left\{ \frac{3}{n \left| \frac{Y_v(u, u_c)}{X_v(u, u_c)} \right| - 2 |\iota(\xi)|}, \frac{3}{n \left| \frac{Y_w(u, u_c)}{X_w(u, u_c)} \right| - 2 |\kappa(\xi)|} \right\}, \quad (55)$$

for all $u > 0$ and $u_c \in [-\|\mathbf{V}_c\|, \|\mathbf{V}_c\|]$.

Proof: The proof is given in Appendix II-E. ■

Theorem 1: The origin $[\tilde{\mathbf{X}}_1^T, \tilde{\mathbf{X}}_2^T] = \mathbf{0}^T$ of the system described by (49),(50) is a USGES equilibrium point if the conditions of Lemmas 2 and 3 hold and the maximum pitch

angle of the path satisfies

$$\theta_{p,\max} = \max_{\xi \in \mathbb{R}} |\theta_p(\xi)| < \frac{\pi}{4}. \quad (56)$$

Moreover, the ocean current estimate errors (51) and the underactuated sway and heave dynamics (52), (53) are bounded.

Remark: Condition (56) is needed to ensure that $|\gamma_{\text{LOS}}| < \pi/2$. Indeed, from (38), the largest possible LOS reference angle is

$$\begin{aligned} \gamma_{\text{LOS},\max} &= \theta_{p,\max} + \lim_{z_b^p \rightarrow \infty} \arctan \left(\frac{z_b^p}{\sqrt{\Delta_0^2 + (z_b^p)^2}} \right) \\ &= \theta_{p,\max} + \frac{\pi}{4}. \end{aligned} \quad (57)$$

With (56) satisfied, the cosine of γ_{LOS} is always positive. We will use this fact in the proof.

Proof: The proof follows along the lines of [9], but is extended to an arbitrary number of 5DOF vehicles. We will also use the results of [10] to prove that the system is USGES.

In Lemmas 1–3, we have shown that the closed-loop system is forward complete and the underactuated sway and heave dynamics are bounded near the manifold $\tilde{\mathbf{X}}_2 = \mathbf{0}$. Since (50) is UGES [11], we can conclude that there exists a finite time $T > t_0$ such that the solutions of (50) will be sufficiently close to $\tilde{\mathbf{X}}_2 = \mathbf{0}$ to guarantee boundedness of v_i and w_i . Having established that the underactuated dynamics are bounded, we will now utilize cascaded theory to analyze the cascade (49), (50), where (50) perturbs the nominal dynamics (49) through the terms $G_y(\cdot)$ and $G_z(\cdot)$.

Now, consider the nominal dynamics of $\tilde{\mathbf{X}}_1$ (*i.e.*, (49) without the perturbing terms G_y and G_z), and a Lyapunov function candidate

$$V(\tilde{\mathbf{X}}_1) = \frac{1}{2} \tilde{\mathbf{X}}_1^T \tilde{\mathbf{X}}_1 = \frac{1}{2} ((x_b^p)^2 + (y_b^p)^2 + (z_b^p)^2), \quad (58)$$

whose derivative along the trajectories of (49) is

$$\dot{V}(\tilde{\mathbf{X}}_1) = -\tilde{\mathbf{X}}_1^T \mathbf{Q} \tilde{\mathbf{X}}_1, \quad \mathbf{Q} = \text{diag}(q_1, q_2, q_3), \quad (59a)$$

$$q_1 = \frac{k_\xi}{\sqrt{1+(x_b^p)^2}}, \quad q_2 = \frac{\frac{1}{n} \sum_{i=1}^n U_{d,i} \cos(\gamma_{\text{LOS}})}{\sqrt{\Delta(\mathbf{p}_b^p)^2 + (y_b^p)^2}}, \quad (59b)$$

$$q_3 = \frac{\frac{1}{n} \sum_{i=1}^n U_{d,i}}{\sqrt{\Delta(\mathbf{p}_b^p)^2 + (z_b^p)^2}}. \quad (59c)$$

Note that \mathbf{Q} is positive definite, and the nominal system is thus UGAS. Furthermore, note that the following inequality

$$\dot{V}(\tilde{\mathbf{X}}_1) \leq -q_{\min} \|\tilde{\mathbf{X}}_1\|^2, \quad (60a)$$

$$q_{\min} = \min \left\{ \frac{k_\xi}{\sqrt{1+r^2}}, \frac{\frac{1}{n} \sum_{i=1}^n U_{d,i} \cos(\gamma_{\text{LOS}})}{\sqrt{\Delta_0^2 + 4r^2}} \right\}, \quad (60b)$$

holds $\forall \tilde{\mathbf{X}}_1 \in \mathcal{B}_r$. Thus, the conditions of [10, Theorem 5] are fulfilled with $k_1 = k_2 = 1/2$, $a = 2$, and $k_3 = q_{\min}$, and the nominal system is USGES.

As discussed in the proof of Lemma 1, the perturbing system (50) is UGES, implying both UGAS and USGES. Furthermore, it is straightforward to show that the following

holds for the Lyapunov function (58)

$$\left\| \frac{\partial V}{\partial \tilde{\mathbf{X}}_1} \right\| \|\tilde{\mathbf{X}}_1\| = \|\tilde{\mathbf{X}}_1\|^2 = 2V(\tilde{\mathbf{X}}_1), \quad \forall \tilde{\mathbf{X}}_1, \quad (61)$$

$$\left\| \frac{\partial V}{\partial \tilde{\mathbf{X}}_1} \right\| = \|\tilde{\mathbf{X}}_1\| \leq \mu, \quad \forall \|\tilde{\mathbf{X}}_1\| \leq \mu. \quad (62)$$

Therefore, [10, Assumption 1] is satisfied with $c_1 = 2$ and $c_2 = \mu$ for any $\mu > 0$.

Finally, [10, Assumption 2] must be investigated. From (82), (92), it can be shown that for both perturbing terms there exist positive functions $\zeta_{y,1}(\cdot)$, $\zeta_{y,2}(\cdot)$, $\zeta_{z,1}(\cdot)$, $\zeta_{z,2}(\cdot)$, such that

$$|G_y(\cdot)| \leq \zeta_{y,1}(\|\tilde{\mathbf{X}}_2\|) + \zeta_{y,2}(\|\tilde{\mathbf{X}}_2\|) \|\tilde{\mathbf{X}}_1\|, \quad (63)$$

$$|G_z(\cdot)| \leq \zeta_{z,1}(\|\tilde{\mathbf{X}}_2\|) + \zeta_{z,2}(\|\tilde{\mathbf{X}}_2\|) \|\tilde{\mathbf{X}}_1\|. \quad (64)$$

Therefore, all conditions of [10, Proposition 9] are satisfied, and the closed-loop system is USGES. ■

VI. SIMULATION RESULTS

In this section, we present the results of a numerical simulation of three LAUV vehicles [16]. The parameters of the simulation are summarized in Table I. The barycenter should follow a spiral path given by

$$\mathbf{p}_p(\xi) = [\xi, a \cos(\omega \xi), b \sin(\omega \xi)]^T. \quad (65)$$

The maximum curvature of this path is

$$\max_{\xi \in \mathbb{R}} |\kappa(\xi)| = \frac{b\omega^2}{\sqrt{a^2\omega^2 + 1}}, \quad \max_{\xi \in \mathbb{R}} |\iota(\xi)| = a\omega^2, \quad (66)$$

while the smallest absolute values of Y_v/X_v and Y_w/X_w for the LAUV model are approximately 0.26. Consequently, the path is chosen such that the maximum curvature is

$$\max_{\xi \in \mathbb{R}} |\kappa(\xi)| = 0.013, \quad \max_{\xi \in \mathbb{R}} |\iota(\xi)| = 0.040, \quad (67)$$

and (54) is satisfied. From (55), the lookahead distance must then satisfy $\Delta_0 > 4.29$. We choose $\Delta_0 = 5$, since smaller distances guarantee faster convergence.

The very minimum relative distance to avoid collision is the length of the LAUV, *i.e.* 2.4 m. For additional safety, we design the COLAV task with $d_{\min} = 5$ m. To add a security zone during transients, d_{COLAV} is chosen to be 10 m.

The desired formation is an isosceles triangle parallel to the yz plane. Specifically, the desired positions of the three vehicles are

$$\mathbf{p}_{f,1}^f = \begin{bmatrix} 0 \\ 10 \\ 5 \end{bmatrix}, \quad \mathbf{p}_{f,2}^f = \begin{bmatrix} 0 \\ -10 \\ 5 \end{bmatrix}, \quad \mathbf{p}_{f,3}^f = \begin{bmatrix} 0 \\ 0 \\ -10 \end{bmatrix}. \quad (68)$$

The gains of the low-level control systems (18),(21),(24) are chosen such that the settling time is approximately 10 seconds. The gains of the pitch and yaw PD controllers are chosen such that the closed-loop system is critically damped.

The results of the numerical simulation are shown in Figures 3 and 4. The vehicles start in an inverted triangular formation. The COLAV task is briefly activated, and the distance between the vehicles drops to approximately 8

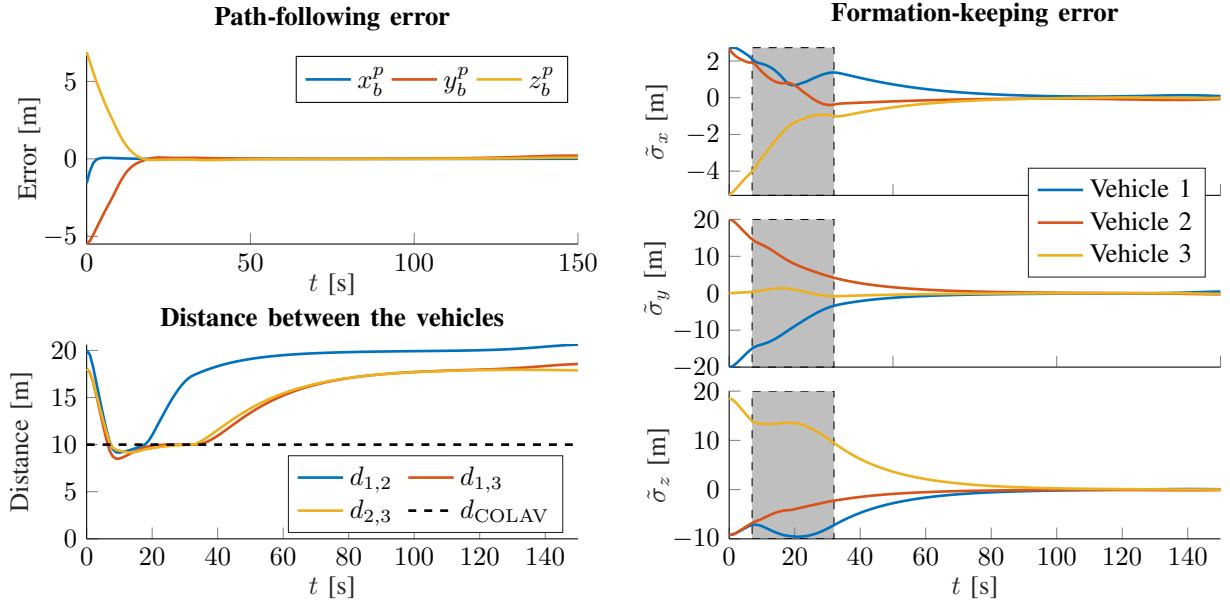


Fig. 3. Simulation results. The top-left plot shows the x -, y - and z -components of the path-following error \mathbf{p}_b^p , as defined in (13). The bottom-left plot shows the distance between the vehicles ($d_{i,j} = \|\mathbf{p}_i - \mathbf{p}_j\|$). The plots on the right show the x -, y - and z -components of the formation-keeping error $\tilde{\sigma} = \sigma_2 - \sigma_{d,2}$ with σ_2 given by (28) and $\sigma_{d,2}$ given by (29). The grey rectangles mark the intervals when the COLAV task is active.

meters during the transient. Eventually, the vehicles resolve the situation and continue to converge to the desired path and formation.

Note that while the COLAV task is active, the formation-keeping error is diverging. After resolving the situation, the formation-keeping error converges to zero exponentially. The rate of convergence is given by the formation-keeping gain Λ_2 .

The path-following error seems to converge linearly at first, and then exponentially as the error gets smaller. This phenomenon is caused by the LOS guidance law (38), cf. [17], and the path parameter update law (46). The inverse tan in (38) and the last term in (46) act as a saturation, slowing the convergence for large errors. The rate of convergence of the along-track error (x_b^p) is given by the path parameter update gain k_ξ , while the rate of convergence of the cross-track errors (y_b^p, z_b^p) is given by the lookahead distance Δ_0 .

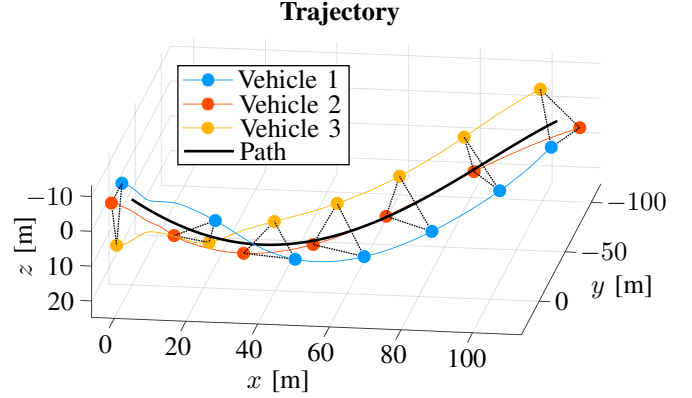


Fig. 4. 3D trajectory of the vehicles. The markers represent the position of the vehicles at times $t = 0, 25, 50, \dots, 150$ seconds. Markers with corresponding times are connected by dotted lines to better illustrate the resulting formation.

VII. CONCLUSIONS AND FUTURE WORK

In this paper, we proposed a formation path-following method for an arbitrary number of AUVs, proved the stability of the path following part, and verified its effectiveness in simulations.

Because the proposed algorithm is centralized, our method can only be used in scenarios where all the vehicles can communicate with each other. A decentralized version of the algorithm is a topic for future work.

In the simulations, the formation-keeping error shows exponential convergence to zero. However, the stability of the formation-keeping task has not been theoretically proven. Proving the stability of this task is another potential topic for future work.

ACKNOWLEDGMENTS

The authors would like to thank Damiano Varagnolo for the interesting discussions and inputs.

Parameter	Value	Parameter	Value
k_u	0.05	\mathbf{V}_c	$[0, 0.25, 0.05]^T$
k_c	0.1	Δ_0	5
k_θ, k_ψ	0.0625	d_{COLAV}	10
k_q, k_r	0.25	U_{LOS}	1
k_d	0.1	k_ξ	1
λ_q, λ_r	0.75	\mathbf{p}_0	$\mathbf{0}_3$
c_u	5	a	40
c_q, c_r	1	b	20
Λ_1	\mathbf{I}	ω	$\pi/100$
Λ_2	$0.05 \mathbf{I}$		

TABLE I
SIMULATION PARAMETERS

This work was partly supported by the Research Council of Norway through project No. 302435 and the Centres of Excellence funding scheme, project No. 223254.

REFERENCES

- [1] B. Das, B. Subudhi, and B. B. Pati, "Cooperative formation control of autonomous underwater vehicles: An overview," *International Journal of Automation and Computing*, vol. 13, no. 3, pp. 199–225, Jun. 2016.
- [2] E. Borhaug and K. Y. Pettersen, "Formation control of 6-DOF Euler-Lagrange systems with restricted inter-vehicle communication," in *Proc. 45th IEEE Conf. Decision and Control*, 2006, pp. 5718–5723.
- [3] R. Ghabcheloo, A. P. Aguiar, A. Pascoal, C. Silvestre, I. Kaminer, and J. Hespanha, "Coordinated path-following control of multiple underactuated autonomous vehicles in the presence of communication failures," in *Proc. 45th IEEE Conference on Decision and Control*, 2006, pp. 4345–4350.
- [4] R. Cui, S. Sam Ge, B. Voon Ee How, and Y. Sang Choo, "Leader-follower formation control of underactuated autonomous underwater vehicles," *Ocean Engineering*, vol. 37, no. 17, pp. 1491–1502, 2010.
- [5] M. Soorki, H. Talebi, and S. Nikravesh, "A robust dynamic leader-follower formation control with active obstacle avoidance," in *Proc. 2011 IEEE International Conference on Systems, Man, and Cybernetics*, 2011, pp. 1932–1937.
- [6] F. Arrichiello, S. Chiaverini, and T. I. Fossen, "Formation control of underactuated surface vessels using the null-space-based behavioral control," in *Proc. 2006 IEEE/RSJ International Conference on Intelligent Robots and Systems*, 2006, pp. 5942–5947.
- [7] G. Antonelli, F. Arrichiello, and S. Chiaverini, "Experiments of formation control with multirobot systems using the null-space-based behavioral control," *IEEE Transactions on Control Systems Technology*, vol. 17, no. 5, pp. 1173–1182, 2009.
- [8] S.-K. Pang, Y.-H. Li, and H. Yi, "Joint formation control with obstacle avoidance of towfish and multiple autonomous underwater vehicles based on graph theory and the null-space-based method," *Sensors*, vol. 19, no. 11, 2019.
- [9] Å. Eek, K. Y. Pettersen, E.-L. M. Ruud, and T. R. Krogstad, "Formation Path Following Control of Underactuated USVs," *European Journal of Control*, Jun. 2021.
- [10] K. Y. Pettersen, "Lyapunov sufficient conditions for uniform semiglobal exponential stability," *Automatica*, vol. 78, pp. 97–102, Apr. 2017.
- [11] S. Moe, K. Y. Pettersen, T. I. Fossen, and J. T. Gravdahl, "Line-of-sight curved path following for underactuated USVs and AUVs in the horizontal plane under the influence of ocean currents," in *Proc. 24th Mediterranean Conf. Control and Automation*, 2016, pp. 38–45.
- [12] T. I. Fossen, *Handbook of Marine Craft Hydrodynamics and Motion Control*. John Wiley & Sons, May 2011.
- [13] E. Borhaug, A. Pavlov, and K. Y. Pettersen, "Straight line path following for formations of underactuated underwater vehicles," in *Proc. 46th IEEE Conf. Decision and Control*, 2007, pp. 2905–2912.
- [14] S. Moe and K. Y. Pettersen, "Set-based line-of-sight (LOS) path following with collision avoidance for underactuated unmanned surface vessels under the influence of ocean currents," in *Proc. 2017 IEEE Conf. Control Technology and Applications*, 2017, pp. 241–248.
- [15] D. Belleter, M. A. Maghenem, C. Paliotta, and K. Y. Pettersen, "Observer based path following for underactuated marine vessels in the presence of ocean currents: A global approach," *Automatica*, vol. 100, pp. 123–134, 2019.
- [16] A. Sousa, L. Madureira, J. Coelho, J. Pinto, J. Pereira, J. Borges Sousa, and P. Dias, "LAUV: The man-portable autonomous underwater vehicle," *IFAC Proceedings Volumes*, vol. 45, no. 5, pp. 268–274, 2012.
- [17] T. I. Fossen and K. Y. Pettersen, "On uniform semiglobal exponential stability (usges) of proportional line-of-sight guidance laws," *Automatica*, vol. 50, no. 11, pp. 2912–2917, 2014.
- [18] D. Angeli and E. D. Sontag, "Forward completeness, unboundedness observability, and their Lyapunov characterizations," *Systems & Control Letters*, vol. 38, no. 4-5, pp. 209–217, 1999.

APPENDIX I
COMPONENTS OF THE DYNAMICAL EQUATIONS

$$F_u(\cdot) = -\frac{d_{11} u + q (m_{34} q + m_{33} w) - r (m_{25} r + m_{22} v)}{m_{11}}, \quad (69a)$$

$$\phi_u(\cdot) = q \left(\frac{m_{33}}{m_{11}} - 1 \right) \mathbf{r}_w + r \left(1 - \frac{m_{22}}{m_{11}} \right) \mathbf{r}_v + \frac{d_{11}}{m_{11}} \mathbf{r}_u, \quad (69b)$$

$$X_v(\cdot) = -u_c - \frac{m_{55} (d_{25} + m_{11} u_r) - m_{25} (d_{55} + m_{25} u_r)}{m_{22} m_{55} - m_{25}^2}, \quad (69c)$$

$$Y_v(\cdot) = -\frac{d_{22} m_{55} - m_{25} (d_{52} - u_r (m_{11} - m_{22}))}{m_{22} m_{55} - m_{25}^2}, \quad (69d)$$

$$X_w(\cdot) = u_c - \frac{m_{44} (d_{34} - m_{11} u_r) - m_{34} (d_{44} - m_{34} u_r)}{m_{33} m_{44} - m_{34}^2}, \quad (69e)$$

$$Y_w(\cdot) = -\frac{d_{33} m_{44} - m_{34} (d_{43} + u_r (m_{11} - m_{33}))}{m_{33} m_{44} - m_{34}^2}, \quad (69f)$$

$$G(\cdot) = \frac{m_{34} m g z_g \sin(\theta)}{m_{33} m_{44} - m_{34}^2}, \quad (69g)$$

$$F_q(\cdot) = \frac{m_{34} (d_{34} q + d_{33} w - q u (m_{11} - m_{33})) - m_{33} (d_{44} q + d_{43} w + m g z_g \sin(\theta) + u w (m_{11} - m_{33}))}{m_{33} m_{44} - m_{34}^2}, \quad (69h)$$

$$\phi_q(\cdot) = \frac{m_{34} (d_{33} \varphi_w - \varphi_u q (m_{11} - m_{33})) - m_{33} (d_{43} \varphi_w + \varphi_{uw} (m_{11} - m_{33}))}{m_{33} m_{44} - m_{34}^2}, \quad (69i)$$

$$F_r(\cdot) = \frac{m_{25} (d_{25} r + d_{22} v + r u (m_{11} - m_{22})) - m_{22} (d_{55} r + d_{52} v - u v (m_{11} - m_{22}))}{m_{22} m_{55} - m_{25}^2}, \quad (69j)$$

$$\phi_r(\cdot) = \frac{m_{25} (d_{22} \varphi_v + \varphi_u r (m_{11} - m_{22})) - m_{22} (d_{52} \varphi_v - \varphi_{uv} (m_{11} - m_{22}))}{m_{22} m_{55} - m_{25}^2}, \quad (69k)$$

where $[\mathbf{r}_u, \mathbf{r}_v, \mathbf{r}_w] = \mathbf{R}(\theta, \psi)$, and

$$\varphi_{ij}(\cdot) = [-j \mathbf{r}_i^T - i \mathbf{r}_j^T, r_{i1} r_{j1}, r_{i2} r_{j2}, r_{i3} r_{j3}, r_{i1} r_{j2} + r_{i2} r_{j1}, r_{i1} r_{j3} + r_{i3} r_{j1}, r_{i2} r_{j3} + r_{i3} r_{j2}]^T, \quad i, j \in \{u, v, w\}. \quad (70)$$

APPENDIX II
DERIVATIONS AND LEMMAS FROM SECTION V

A. Derivation of Closed-Loop Barycenter Kinematics

We begin by taking \dot{y}_b^p from (44b).

$$\dot{y}_b^p = \frac{1}{n} \sum_{i=1}^n U_i \cos(\gamma_i) \sin(\chi_i - \psi_p) - \dot{\xi}^t x_b^p. \quad (71)$$

Now, consider the term $\sin(\chi_i - \psi_p)$. The course of the vessel is given by

$$\chi_i = \psi_i + \beta_i, \quad \beta_i = \arcsin\left(\frac{v_i}{U_i}\right). \quad (72)$$

After substituting and applying some trigonometric identities, we get

$$\sin(\chi_i - \psi_p) = \sin(\psi_i + \beta_i - \psi_p) = \cos(\psi_i - \psi_p) \sin(\beta_i) + \sin(\psi_i - \psi_p) \cos(\beta_i) \quad (73a)$$

$$= \cos(\psi_i - \psi_p) \frac{v_i}{U_i} + \sin(\psi_i - \psi_p) \frac{\sqrt{u_i^2 + w_i^2}}{U_i}. \quad (73b)$$

Consequently, the term $U_i \cos(\gamma_i) \sin(\chi_i - \psi_p)$ is equivalent to

$$U_i \cos(\gamma_i) \sin(\chi_i - \psi_p) = \cos(\gamma_i) \left(\cos(\psi_i - \psi_p) v_i + \sin(\psi_i - \psi_p) \sqrt{u_i^2 + w_i^2} \right). \quad (74)$$

Now, consider a term $\sin(\psi_i + \beta_{d,i} - \psi_p)$. Using a similar procedure, we get

$$\sin(\psi_i + \beta_{d,i} - \psi_p) = \cos(\psi_i - \psi_p) \frac{v_i}{U_{d,i}} + \sin(\psi_i - \psi_p) \frac{\sqrt{u_{d,i}^2 + w_i^2}}{U_{d,i}}. \quad (75)$$

Combining (74) and (75), we get

$$U_i \cos(\gamma_i) \sin(\chi_i - \psi_p) = U_{d,i} \cos(\gamma_i) \sin(\psi_i + \beta_{d,i} - \psi_p) + \cos(\gamma_i) \sin(\psi_i - \psi_p) \left(\sqrt{u_i^2 + w_i^2} - \sqrt{u_{d,i}^2 + w_i^2} \right). \quad (76)$$

Note that the following holds for the angles

$$\psi_i + \beta_{d,i} - \psi_p = \psi_{d,i} + \tilde{\psi}_i + \beta_{d,i} - (\psi_{d,i} + \beta_{d,i} + \beta_{\text{LOS}}) = \tilde{\psi}_i - \beta_{\text{LOS}}, \quad \beta_{\text{LOS}} = \arctan\left(\frac{y_b^p}{\Delta(\mathbf{p}_b^p)}\right). \quad (77)$$

Therefore, their sine is given by

$$\sin(\psi_i + \beta_{d,i} - \psi_p) = \sin(\tilde{\psi}_i) \frac{\Delta(\mathbf{p}_b^p)}{\sqrt{\Delta(\mathbf{p}_b^p)^2 + (y_b^p)^2}} - \cos(\tilde{\psi}_i) \frac{y_b^p}{\sqrt{\Delta(\mathbf{p}_b^p)^2 + (y_b^p)^2}}. \quad (78)$$

Furthermore, note that the following holds for the flight-path angle

$$\gamma_i = \theta_i - \alpha_i = \tilde{\theta}_i + \theta_{d,i} - \alpha_i = \tilde{\theta}_i + \gamma_{\text{LOS}} + \alpha_{d,i} - \alpha_i. \quad (79)$$

Consequently, the cosine of the flight-path angle is equal to

$$\begin{aligned} \cos(\gamma_i) &= \cos(\gamma_{\text{LOS}}) \cos(\tilde{\theta}_i) \cos(\alpha_{d,i} - \alpha_i) - \cos(\gamma_{\text{LOS}}) \sin(\tilde{\theta}_i) \sin(\alpha_{d,i} - \alpha_i) \\ &\quad - \sin(\gamma_{\text{LOS}}) \cos(\tilde{\theta}_i) \sin(\alpha_{d,i} - \alpha_i) - \sin(\gamma_{\text{LOS}}) \sin(\tilde{\theta}_i) \cos(\alpha_{d,i} - \alpha_i) \end{aligned} \quad (80)$$

Using the equalities (78), (80), we can rewrite (76) as

$$U_i \cos(\gamma_i) \sin(\chi_i - \psi_p) = -U_{d,i} \cos(\gamma_{\text{LOS}}) \frac{y_b^p}{\sqrt{\Delta(\mathbf{p}_b^p)^2 + (y_b^p)^2}} + G_{y,i}(\tilde{u}_i, \tilde{\psi}_i, \gamma_i, u_{d,i}, v_i, w_i, \mathbf{p}_b^p, \psi_p), \quad (81)$$

where

$$\begin{aligned} G_{y,i}(\cdot) &= \cos(\gamma_i) \sin(\psi_i - \psi_p) \left(\sqrt{u_i^2 + w_i^2} - \sqrt{u_{d,i}^2 + w_i^2} \right) - U_{d,i} \cos(\gamma_i) \sin(\tilde{\psi}_i) \frac{\Delta(\mathbf{p}_b^p)}{\sqrt{\Delta(\mathbf{p}_b^p)^2 + (y_b^p)^2}} \\ &\quad + U_{d,i} \left[\sin(\gamma_{\text{LOS}}) \left(\cos(\tilde{\theta}_i) \sin(\alpha_{d,i} - \alpha_i) + \sin(\tilde{\theta}_i) \cos(\alpha_{d,i} - \alpha_i) \right) \right. \\ &\quad \left. - \cos(\gamma_{\text{LOS}}) \left(\cos(\tilde{\theta}_i) \cos(\alpha_{d,i} - \alpha_i) - 1 \right) \right] \frac{y_b^p}{\sqrt{\Delta(\mathbf{p}_b^p)^2 + (y_b^p)^2}} \end{aligned} \quad (82)$$

Substituting (81) into (71), we get the following

$$\begin{aligned} \dot{y}_b^p &= -\frac{1}{n} \sum_{i=1}^n U_{d,i} \cos(\gamma_{\text{LOS}}) \frac{y_b^p}{\sqrt{\Delta(\mathbf{p}_b^p)^2 + (y_b^p)^2}} - \dot{\xi} \iota x_b^p \\ &\quad + G_y(\tilde{u}_1, \dots, \tilde{u}_n, \tilde{\psi}_1, \dots, \tilde{\psi}_n, \gamma_1, \dots, \gamma_n, u_{d,1}, \dots, u_{d,n}, v_1, \dots, v_n, w_1, \dots, w_n, \mathbf{p}_b^p, \psi_p), \end{aligned} \quad (83)$$

where

$$G_y(\cdot) = \frac{1}{n} \sum_{i=1}^n G_{y,i}(\tilde{u}_i, \tilde{\psi}_i, \gamma_i, u_{d,i}, v_i, w_i, \mathbf{p}_b^p, \psi_p). \quad (84)$$

Now, we demonstrate a similar procedure for \dot{z}_b^p . From (44b), we get

$$\dot{z}_b^p = \frac{1}{n} \sum_{i=1}^n U_i (-\cos(\theta_p) \sin(\gamma_i) + \cos(\gamma_i) \sin(\theta_p) \cos(\psi_p - \chi_i)) + \dot{\xi} \kappa x_b^p \quad (85a)$$

$$= \frac{1}{n} \sum_{i=1}^n U_i (-\sin(\gamma_i - \theta_p) - (1 - \cos(\chi_i - \psi_p)) \cos(\gamma_i) \sin(\theta_p)) + \dot{\xi} \kappa x_b^p. \quad (85b)$$

Once again, we consider the terms

$$\sin(\gamma_i - \theta_p) = \sin(\theta_i - \alpha_i - \theta_p) = \sin(\theta_i - \theta_p) \frac{u_i}{U_i} - \cos(\theta_i - \theta_p) \frac{w_i}{U_i}, \quad (86)$$

and

$$\sin(\theta_i - \alpha_{d,i} - \theta_p) = \sin(\theta_i - \theta_p) \frac{u_{d,i}}{U_{d,i}} - \cos(\theta_i - \theta_p) \frac{w_i}{U_{d,i}}, \quad (87)$$

which give us the following equality

$$U_i \sin(\gamma_i - \theta_p) = U_{d,i} \sin(\theta_i - \alpha_{d,i} - \theta_p) + \tilde{u}_i \sin(\theta_i - \theta_p). \quad (88)$$

Using a similar trick, we can write the sine as

$$\sin(\theta_i - \alpha_{d,i} - \theta_p) = \sin(\tilde{\theta}_i - \alpha_{\text{LOS}}) = \sin(\tilde{\theta}_i) \frac{\Delta(\mathbf{p}_b^p)}{\sqrt{\Delta(\mathbf{p}_b^p)^2 + (z_b^p)^2}} - \cos(\tilde{\theta}_i) \frac{(z_b^p)}{\sqrt{\Delta(\mathbf{p}_b^p)^2 + (z_b^p)^2}} \quad (89)$$

Consequently, we can rewrite (85b) as

$$\begin{aligned} \dot{z}_b^p &= -\frac{1}{n} \sum_{i=1}^n U_{d,i} \frac{z_b^p}{\sqrt{\Delta(\mathbf{p}_b^p)^2 + (z_b^p)^2}} + \dot{\xi} \kappa x_b^p \\ &+ G_z(\tilde{u}_1, \dots, \tilde{u}_n, \tilde{\theta}_1, \dots, \tilde{\theta}_n, \gamma_1, \dots, \gamma_n, \chi_1, \dots, \chi_n, u_{d,1}, \dots, u_{d,n}, v_1, \dots, v_n, w_1, \dots, w_n, \mathbf{p}_b^p, \theta_p, \psi_p), \end{aligned} \quad (90)$$

where

$$G_z(\cdot) = \frac{1}{n} \sum_{i=1}^n G_{z,i}(\tilde{u}_i, \tilde{\theta}_i, \gamma_i, \chi_i, u_{d,i}, v_i, w_i, \mathbf{p}_b^p, \theta_p, \psi_p), \quad (91)$$

$$\begin{aligned} G_{z,i}(\cdot) &= -U_i((1 - \cos(\chi_i - \psi_p)) \cos(\gamma_i) \sin(\theta_p)) - \tilde{u}_i \sin(\theta_i - \theta_p) \\ &- (1 - \cos(\tilde{\theta}_i)) \frac{(z_b^p)}{\sqrt{\Delta(\mathbf{p}_b^p)^2 + (z_b^p)^2}} - U_{d,i} \sin(\tilde{\theta}_i) \frac{\Delta(\mathbf{p}_b^p)}{\sqrt{\Delta(\mathbf{p}_b^p)^2 + (z_b^p)^2}}. \end{aligned} \quad (92)$$

B. Desired Pitch and Yaw Rate

For further calculations, we need to evaluate the desired pitch ($q_{d,i}$) and yaw ($r_{d,i}$) rates of the vessels. From (11d), we get the following relation between the yaw rate and the derivative of the yaw angle

$$q_{d,i} = \dot{\theta}_{d,i}. \quad (93)$$

Now, we consider the desired pitch angle from (35). Since we are investigating the path following task, we substitute γ_{LOS} from (38) for $\gamma_{\text{NSB},i}$. Differentiating (35) with respect to time yields

$$q_{d,i} = \dot{\theta}_p(\xi) + \frac{\Delta(\mathbf{p}_b^p) \dot{z}_b^p - z_b^p \dot{\Delta}(\mathbf{p}_b^p)}{\Delta(\mathbf{p}_b^p)^2 + (z_b^p)^2} + \frac{u_{d,i} \dot{w}}{u_{d,i}^2 + w_i^2} \quad (94a)$$

$$\begin{aligned} &= \dot{\xi} \kappa(\xi) + \frac{\Delta(\mathbf{p}_b^p) \left(\frac{1}{n} \sum_{j=1}^n U_{d,j} \frac{(z_b^p)}{\sqrt{\Delta(\mathbf{p}_b^p)^2 + (z_b^p)^2}} + \dot{\xi} \kappa x_b^p + G_z(\cdot) \right)}{\Delta(\mathbf{p}_b^p)^2 + (z_b^p)^2} \\ &+ \frac{z_b^p \left(-k_\xi \frac{(x_b^p)^2}{\sqrt{1+(x_b^p)^2}} - \frac{1}{n} \sum_{j=1}^n U_{d,j} \left(\frac{\cos(\gamma_{\text{LOS},j})^2 (y_b^p)^2}{\sqrt{\Delta(\mathbf{p}_b^p)^2 + (y_b^p)^2}} + \frac{(z_b^p)^2}{\sqrt{\Delta(\mathbf{p}_b^p)^2 + (z_b^p)^2}} \right) + y_b^p G_y(\cdot) + z_b^p G_z(\cdot) \right)}{\Delta(\mathbf{p}_b^p) (\Delta(\mathbf{p}_b^p)^2 + (z_b^p)^2)} \\ &+ u_{d,i} \frac{X_w(u_{d,i} + \tilde{u}_i, u_c) q + Y_w(u_{d,i} + \tilde{u}_i, u_c) (w_i - w_c)}{u_{d,i}^2 + w_i^2}. \end{aligned} \quad (94b)$$

From (11e), we get the following relation between the yaw rate and the derivative of the yaw angle

$$r_{d,i} = \dot{\psi}_{d,i} \cos(\theta_{d,i}). \quad (95)$$

Substituting the time-derivative of (36), we get

$$r_{d,i} = \left(\dot{\psi}_p(\xi) - \frac{\Delta(\mathbf{p}_b^p) \dot{y}_b^p - y_b^p \dot{\Delta}(\mathbf{p}_b^p)}{\Delta(\mathbf{p}_b^p)^2 + (y_b^p)^2} - \frac{\dot{v}}{\sqrt{U_{d,i}^2 - v_i^2}} \right) \cos(\theta_{d,i}) \quad (96a)$$

$$\begin{aligned}
&= \left(\begin{aligned} &\xi \iota(\xi) - \frac{\Delta(\mathbf{p}_b^p) \left(\frac{1}{n} \sum_{j=1}^n U_{d,i} \frac{\cos(\gamma_{\text{LOS}})(y_b^p)}{\sqrt{\Delta(\mathbf{p}_b^p)^2 + (y_b^p)^2}} - \xi \iota x_b^p + G_y(\cdot) \right)}{\Delta(\mathbf{p}_b^p)^2 + (y_b^p)^2} \\ &+ \frac{y_b^p \left(-k_\xi \frac{(x_b^p)^2}{\sqrt{1+(x_b^p)^2}} - \frac{1}{n} \sum_{j=1}^n U_{d,i} \left(\frac{\cos(\gamma_{\text{LOS}})^2 (y_b^p)^2}{\sqrt{\Delta(\mathbf{p}_b^p)^2 + (y_b^p)^2}} + \frac{(z_b^p)^2}{\sqrt{\Delta(\mathbf{p}_b^p)^2 + (z_b^p)^2}} \right) + y_b^p G_y(\cdot) + z_b^p G_z(\cdot) \right)}{\Delta(\mathbf{p}_b^p) \left(\Delta(\mathbf{p}_b^p)^2 + (y_b^p)^2 \right)} \\ &- \frac{X(u_{d,i} + \tilde{u}_i, u_c) r + Y(u_{d,i} + \tilde{u}_i, u_c) (v_i - v_c)}{\sqrt{u_{d,i}^2 + w_i^2}} \end{aligned} \right) \cos(\theta_{d,i}). \quad (96b)
\end{aligned}$$

C. Proof of Lemma 1

In [11], it is shown that the error states (50a)–(50e) are UGES and the ocean current estimate errors (51a)–(51c) are bounded, which implies that (50a)–(51c) are forward complete. Therefore, we only need to prove that the underactuated sway and heave dynamics (52), (53) and the barycenter dynamics (49a)–(49c) are forward complete.

First, let us consider the underactuated sway dynamics. From (52), we get

$$\dot{v}_i = X_v(\tilde{u}_i + u_{d,i}, u_c) (\tilde{r}_i + r_{d,i}) + Y_v(\tilde{u}_i + u_{d,i}, u_c) (v_i - v_c), \quad (97)$$

where $\tilde{r}_i = r_i - r_{d,i}$. Now, let us consider a Lyapunov function candidate

$$V_v(v_i) = \frac{1}{2} v_i^2. \quad (98)$$

Its derivative along the trajectories of v_i is

$$\dot{V}_v(v_i) = X_v(\tilde{u}_i + u_{d,i}, u_c) (\tilde{r}_i + r_{d,i}) v_i + Y_v(\tilde{u}_i + u_{d,i}, u_c) (v_i - v_c) v_i. \quad (99)$$

From the boundedness of $\tilde{\mathbf{X}}_{2,i}$, $\kappa(\xi)$, $\iota(\xi)$, $u_{d,i}$, u_c and v_c , we can conclude that there exists some scalar $\beta_{v,0} > 0$ such that $\left\| \left[\tilde{\mathbf{X}}_{2,i}^T, \kappa(\xi), \iota(\xi), u_{d,i}, u_c, v_c \right]^T \right\| \leq \beta_0$. Moreover, from (96), we can conclude that there exist some positive functions $a_r(\beta_{v,0})$ and $b_r(\beta_{v,0})$ such that

$$|r_{d,i}| \leq a_r(\beta_{v,0}) |v_i| + b_r(\beta_{v,0}). \quad (100)$$

Consequently, we can upper bound $\dot{V}_v(v_i)$ using the following expression

$$\dot{V}_v(v_i) \leq X_v(\tilde{u}_i + u_{d,i}, u_c) (\tilde{r}_i v_i + a_r(\cdot) v_i^2 + b_r(\cdot) v_i) + Y_v(\tilde{u}_i + u_{d,i}, u_c) (v_i^2 - v_c v_i). \quad (101)$$

Using Young's inequality, we get

$$\begin{aligned} \dot{V}_v(v_i) &\leq (X_v(\tilde{u}_i + u_{d,i}, u_c) (2 + a_r(\cdot)) + 2 Y_v(\tilde{u}_i + u_{d,i}, u_c)) v_i^2 \\ &\quad + X_v(\tilde{u}_i + u_{d,i}, u_c) (\tilde{r}_i^2 + b_r(\cdot)^2) + Y_v(\tilde{u}_i + u_{d,i}, u_c) v_c^2 \end{aligned} \quad (102a)$$

$$\leq \alpha_v V_v(v_i) + \beta_v. \quad (102b)$$

Using the comparison lemma, we get

$$V_v(v_i(t)) \leq \left(V_v(v_i(t_0)) + \frac{\beta_v}{\alpha_v} \right) \exp(\alpha_v(t - t_0)) - \frac{\beta_v}{\alpha_v}. \quad (103)$$

As $V_v(v_i)$ is defined for all $t > t_0$, it follows that v_i is also defined for all $t > t_0$. The solutions of (52) thus fulfill the definition of forward completeness, as defined in [18].

Now, let us consider the underactuated heave dynamics. From (53), we get

$$\dot{w}_i = X_w(\tilde{u}_i + u_{d,i}, u_c) (\tilde{q}_i + q_{d,i}) + Y_w(\tilde{u}_i + u_{d,i}, u_c) (w_i - w_c) + G(\theta_i), \quad (104)$$

where $\tilde{q}_i = q_i - q_{d,i}$. Similar to the previous paragraph, we consider a Lyapunov function candidate

$$V_w(w_i) = \frac{1}{2} w_i^2, \quad (105)$$

whose derivative is

$$\dot{V}_w(w_i) = X_w(\tilde{u}_i + u_{d,i}, u_c) (\tilde{q}_i + q_{d,i}) w_i + Y_w(\tilde{u}_i + u_{d,i}, u_c) (w_i - w_c) w_i + G(\theta) w_i. \quad (106)$$

From the boundedness of $\tilde{\mathbf{X}}_{2,i}$, $\kappa(\xi)$, $\iota(\xi)$, $u_{d,i}$, u_c and w_c , we can conclude that there exists some scalar $\beta_0 > 0$ such that $\left\| \left[\tilde{\mathbf{X}}_{2,i}^T, \kappa(\xi), \iota(\xi), u_{d,i}, u_c, w_c \right]^T \right\| \leq \beta_{w,0}$. Moreover, from (94), we can conclude that there exist some positive functions $a_q(\beta_{w,0})$ and $b_q(\beta_{w,0})$ such that

$$|q_{d,i}| \leq a_q(\beta_{w,0}) |w_i| + b_q(\beta_{w,0}). \quad (107)$$

Consequently, we can upper bound $\dot{V}_w(w_i)$ using the following expression

$$\dot{V}_w(w_i) \leq X_w(\tilde{u}_i + u_{d,i}, u_c) (\tilde{q}_i w_i + a_q(\cdot) w_i^2 + b_q(\cdot) w_i) + Y_w(\tilde{u}_i + u_{d,i}, u_c) (w_i^2 - w_c w_i) + G(\theta) w_i. \quad (108)$$

Using Young's inequality, we get

$$\dot{V}_w(w_i) \leq (X_w(\tilde{u}_i + u_{d,i}, u_c) (2 + a_q(\cdot)) + 2 Y_w(\tilde{u}_i + u_{d,i}, u_c) + 1) w_i^2 \quad (109a)$$

$$+ X_w(\tilde{u}_i + u_{d,i}, u_c) (\tilde{q}_i^2 + b_q(\cdot)^2) + Y_w(\tilde{u}_i + u_{d,i}, u_c) w_c^2 + G(\theta)^2 \leq \alpha_w V_w(w_i) + \beta_w. \quad (109b)$$

Using the comparison lemma, we get

$$V_w(w_i(t)) \leq \left(V_w(w_i(t_0)) + \frac{\beta_w}{\alpha_w} \right) \exp(\alpha_w(t - t_0)) - \frac{\beta_w}{\alpha_w}. \quad (110)$$

Using the same arguments as in the previous paragraph, we conclude that the solutions of (53) are forward complete.

Finally, let us consider the barycenter dynamics. We use a Lyapunov function candidate

$$V_b(\mathbf{p}_b^p) = \frac{1}{2} \left((x_b^p)^2 + (y_b^p)^2 + (z_b^p)^2 \right), \quad (111)$$

whose derivative along the solutions of (49a)–(49c) is

$$\dot{V}_b(\mathbf{p}_b^p) = -k_\xi \frac{(x_b^p)^2}{\sqrt{1 + (x_b^p)^2}} - \frac{1}{n} \sum_{i=1}^n U_{d,i} \left(\frac{\cos(\gamma_{\text{LOS}})^2 (y_b^p)^2}{\sqrt{\Delta(\mathbf{p}_b^p)^2 + (y_b^p)^2}} + \frac{(z_b^p)^2}{\sqrt{\Delta(\mathbf{p}_b^p)^2 + (z_b^p)^2}} \right) + G_y(\cdot) y_b^p + G_z(\cdot) z_b^p \quad (112a)$$

$$\leq G_y(\cdot) y_b^p + G_z(\cdot) z_b^p + \frac{1}{2} (x_b^p)^2. \quad (112b)$$

Using Young's inequality, we get

$$\dot{V}_b(\mathbf{p}_b^p) \leq \frac{1}{2} \left((x_b^p)^2 + (y_b^p)^2 + (z_b^p)^2 \right) + \frac{1}{2} (G_y(\cdot)^2 + G_z(\cdot)^2) = V_b(\mathbf{p}_b^p) + \frac{1}{2} (G_y(\cdot)^2 + G_z(\cdot)^2). \quad (113)$$

Note that from (82) and (92), we can conclude that there exist some positive function $\zeta_y(U_{d,1}, \dots, U_{d,n})$ and $\zeta_z(U_{d,1}, \dots, U_{d,n})$ such that

$$|G_y(\cdot)| \leq \zeta_y(\cdot) \left\| \left[\tilde{u}_1, \dots, \tilde{u}_n, \tilde{\psi}_1, \dots, \tilde{\psi}_n \right]^T \right\|, \quad (114)$$

$$|G_z(\cdot)| \leq \zeta_z(\cdot) \left\| \left[\tilde{u}_1, \dots, \tilde{u}_n, \tilde{\theta}_1, \dots, \tilde{\theta}_n \right]^T \right\|. \quad (115)$$

$$(116)$$

Consequently, there exists a class- \mathcal{K}_∞ function $\zeta_p(\cdot)$ such that

$$\dot{V}_p(\mathbf{p}_b^p) \leq V_p(\mathbf{p}_b^p) + \zeta_p \left(v_1, \dots, v_n, w_1, \dots, w_n, \tilde{u}_1, \dots, \tilde{u}_n, \tilde{\psi}_1, \dots, \tilde{\psi}_n, \tilde{\theta}_1, \dots, \tilde{\theta}_n \right). \quad (117)$$

Since all the arguments of $\zeta_p(\cdot)$ are forward complete, Corollary 2.11 of [18] is satisfied and the barycenter dynamics is forward complete, thus concluding the proof of Lemma 1.

D. Proof of Lemma 2

First, we consider the sway dynamics. We take the Lyapunov function candidate V_v from (98) and simplify its derivative by setting $\left[\tilde{\mathbf{X}}_1^T, \tilde{\mathbf{X}}_2^T \right] = \mathbf{0}^T$.

$$\dot{V}_v(v_i) = X_v(u_{d,i}, u_c) r_{d,i} v_i + Y_v(u_{d,i}, u_c) (v_i - v_c) v_i. \quad (118)$$

Next, we find an upper bound on $r_{d,i} v_i$. We substitute from (96), set $[\tilde{\mathbf{X}}_1^T, \tilde{\mathbf{X}}_2^T] = \mathbf{0}^T$ and collect all terms that grow linearly with v_i to obtain the following expression

$$r_{d,i} v_i = \left(v_i \left(1 + \frac{\Delta(\mathbf{p}_b^p) x_b^p}{\Delta(\mathbf{p}_b^p)^2 + (x_b^p)^2} \right) \iota(\xi) \frac{1}{n} \sum_{j=1}^n U_j \Omega_x(\gamma_j, \theta_p, \chi_j, \psi_p) + \frac{Y_v(u_{d,i}, u_c)}{\sqrt{u_{d,i}^2 + w_i^2}} v_i^2 \right) \cos(\theta_{d,i}) + F_v(u_{d,i}, \theta_{d,i}, u_c, v_c, v_i, w_i, r_i), \quad (119)$$

$$F_v(\cdot) = \frac{X_v(u_{d,i}, u_c) r_i - Y_v(u_{d,i}, u_c) v_c}{\sqrt{u_{d,i}^2 + w_i^2}} v_i \cos(\theta_{d,i}). \quad (120)$$

We can bound this expression as

$$|r_{d,i} v_i| \leq \frac{2}{n} |v_i| |\iota(\xi)| \sum_{j=1}^n (|u_j| + |v_j| + |w_j|) + |F_v(\cdot)| \quad (121a)$$

$$\leq \frac{2}{n} |\iota(\xi)| v_i^2 + \frac{2}{n} |v_i| |\iota(\xi)| \left(\sum_{j \in \{1, \dots, n\} \setminus \{i\}} (|u_j| + |v_j| + |w_j|) + |u_i| + |w_i| \right) + |F_v(\cdot)|, \quad (121b)$$

which we can substitute to (118) to obtain

$$\begin{aligned} \dot{V}_v(v_i) &\leq \left(X_v(u_{d,i}, u_c) \frac{2}{n} |\iota(\xi)| + Y_v(u_{d,i}, u_c) \right) v_i^2 + \left(\frac{2}{n} |v_i| |\iota(\xi)| \sum_{j \in \{1, \dots, n\} \setminus \{i\}} (|u_j| + |v_j| + |w_j|) + |u_i| + |w_i| \right) \\ &\quad + (|F_v(\cdot)| - Y_v(u_{d,i}, u_c) |v_c|) |v_i|. \end{aligned} \quad (122)$$

For a sufficiently large v_i , the quadratic term will dominate the linear term. Therefore, we can conclude that v_i is bounded if

$$X_v(u_{d,i}, u_c) \frac{2}{n} |\iota(\xi)| + Y_v(u_{d,i}, u_c) < 0. \quad (123)$$

Since Y_v is assumed to be always negative, the inequality is satisfied if

$$|\iota(\xi)| < \frac{n}{2} \left| \frac{Y_v(u_{d,i}, u_c)}{X_v(u_{d,i}, u_c)} \right|. \quad (124)$$

Now, we perform a similar procedure for the heave dynamics. We take the Lyapunov function candidate V_w from (105) and simplify its derivative by setting $[\tilde{\mathbf{X}}_1^T, \tilde{\mathbf{X}}_2^T] = \mathbf{0}^T$.

$$\dot{V}_w(w_i) = X_w(u_{d,i}, u_c) q_{d,i} w_i + Y_w(u_{d,i}, u_c) (w_i - w_c) w_i + G(\theta_i) w_i. \quad (125)$$

Next, we find an upper bound on $q_{d,i} w_i$. We substitute from (94), set $[\tilde{\mathbf{X}}_1^T, \tilde{\mathbf{X}}_2^T] = \mathbf{0}^T$ and collect all terms that grow linearly with w_i to obtain the following expression

$$q_{d,i} w_i = w_i \left(1 + \frac{\Delta(\mathbf{p}_b^p) x_b^p}{\Delta(\mathbf{p}_b^p)^2 + (x_b^p)^2} \right) \kappa(\xi) \frac{1}{n} \sum_{j=1}^n U_j \Omega_x(\gamma_j, \theta_p, \chi_j, \psi_p) + u_{d,i} \frac{Y_w(u_{d,i}, u_c)}{\sqrt{u_{d,i}^2 + w_i^2}} w_i^2 + F(u_{d,i}, u_c, w_c, w_i, q_i), \quad (126)$$

$$F(\cdot) = u_{d,i} \frac{X_w(u_{d,i}, u_c) r_i - Y_w(u_{d,i}, u_c) w_c}{\sqrt{u_{d,i}^2 + w_i^2}} w_i. \quad (127)$$

We can bound this expression as

$$|q_{d,i} w_i| \leq \frac{2}{n} |\kappa(\xi)| w_i^2 + \frac{2}{n} |w_i| |\kappa(\xi)| \left(\sum_{j \in \{1, \dots, n\} \setminus \{i\}} (|u_j| + |v_j| + |w_j|) + |u_i| + |v_i| \right) + |F(\cdot)|, \quad (128a)$$

which we can substitute to (125) to obtain

$$\begin{aligned} \dot{V}_w(w_i) &\leq \left(X_w(u_{d,i}, u_c) \frac{2}{n} |\kappa(\xi)| + Y_w(u_{d,i}, u_c) \right) w_i^2 + \left(\frac{2}{n} |w_i| |\kappa(\xi)| \sum_{j \in \{1, \dots, n\} \setminus \{i\}} (|u_j| + |v_j| + |w_j|) + |u_i| + |w_i| \right) \\ &\quad + (|F(\cdot)| - Y_w(u_{d,i}, u_c) |v_c| + |G(\theta_i)|) |w_i| + G(\theta_i) w_i. \end{aligned} \quad (129)$$

For a sufficiently large w_i , the quadratic term will dominate the linear term. Therefore, we can conclude that w_i is bounded if

$$X_w(u_{d,i}, u_c) \frac{2}{n} |\kappa(\xi)| + Y_w(u_{d,i}, u_c) < 0. \quad (130)$$

Since Y_w is assumed to be always negative, the inequality is satisfied if

$$|\kappa(\xi)| < \frac{n}{2} \left| \frac{Y_w(u_{d,i}, u_c)}{X_w(u_{d,i}, u_c)} \right|, \quad (131)$$

which concludes the proof of Lemma 2.

E. Proof of Lemma 3

First, we consider the sway dynamics. We take the Lyapunov function candidate V_v from (98) and simplify its derivative by setting $\tilde{\mathbf{X}}_2 = \mathbf{0}$.

$$\dot{V}_v(v_i) = X_v(u_{d,i}, u_c) r_{d,i} v_i + Y_v(u_{d,i}, u_c) (v_i - v_c) v_i. \quad (132)$$

Next, we find an upper bound on $r_{d,i} v_i$. We substitute from (96), set $\tilde{\mathbf{X}}_2 = \mathbf{0}$ and collect all terms that grow linearly with v_i to obtain the following expression

$$\begin{aligned} r_{d,i} v_i = & \left(v_i \left(1 + \frac{\Delta(\mathbf{p}_b^p) x_b^p}{\Delta(\mathbf{p}_b^p)^2 + (x_b^p)^2} \right) \iota(\xi) \frac{1}{n} \sum_{j=1}^n U_j \Omega_x(\gamma_j, \theta_p, \chi_j, \psi_p) - \frac{y_b^p v_i \sum_{j=1}^n \left(\frac{\cos(\gamma_{\text{LOS}}) y_b^p}{\sqrt{\Delta(\mathbf{p}_b^p)^2 + (y_b^p)^2}} + \frac{z_b^p}{\sqrt{\Delta(\mathbf{p}_b^p)^2 + (z_b^p)^2}} \right)}{n \Delta(\mathbf{p}_b^p) (\Delta(\mathbf{p}_b^p)^2 + (y_b^p)^2)} \right. \\ & \left. + \frac{v_i \Delta(\mathbf{p}_b^p) \sum_{j=1}^n \frac{\cos(\gamma_{\text{LOS}}) y_b^p}{\sqrt{\Delta(\mathbf{p}_b^p)^2 + (y_b^p)^2}}}{n (\Delta(\mathbf{p}_b^p)^2 + (y_b^p)^2)} + \frac{Y_v(u_{d,i}, u_c)}{\sqrt{u_{d,i}^2 + w_i^2}} v_i^2 \right) \cos(\theta_{d,i}) + H_v(u_{d,i}, \theta_{d,i}, u_c, v_c, v_i, w_i, r_i, \mathbf{p}_b^p, \xi), \end{aligned} \quad (133)$$

$$\begin{aligned} H_v(\cdot) = & \left(\left(1 + \frac{\Delta(\mathbf{p}_b^p) x_b^p}{\Delta(\mathbf{p}_b^p)^2 + (x_b^p)^2} \right) k_\xi \iota(\xi) \frac{x_b^p}{\sqrt{1 + (x_b^p)^2}} - \frac{y_b^p k_\xi x_b^p}{\sqrt{1 + (x_b^p)^2} \Delta(\mathbf{p}_b^p) (\Delta(\mathbf{p}_b^p)^2 + (y_b^p)^2)} \right. \\ & \left. + \frac{X_v(u_{d,i}, u_c) r_i - Y_v(u_{d,i}, u_c) v_c}{\sqrt{u_{d,i}^2 + w_i^2}} \right) v_i \cos(\theta_{d,i}). \end{aligned} \quad (134)$$

We can bound this expression as

$$|r_{d,i} v_i| \leq \left(\frac{2}{n} |\iota(\xi)| + \frac{3}{n \Delta(\mathbf{p}_b^p)} \right) |v_i| \sum_{j=1}^n (|u_j| + |v_j| + |w_j|) + |H_v(\cdot)| \quad (135a)$$

$$\leq \left(\frac{2}{n} |\iota(\xi)| + \frac{3}{n \Delta(\mathbf{p}_b^p)} \right) v_i^2 + \left(\frac{2}{n} |\iota(\xi)| + \frac{3}{n \Delta(\mathbf{p}_b^p)} \right) \left(\sum_{j \in \{1, \dots, n\} \setminus \{i\}} (|u_j| + |v_j| + |w_j|) + |u_i| + |w_i| \right) \quad (135b)$$

$$+ |H_v(\cdot)|, \quad (135c)$$

which we can substitute to (132) to obtain

$$\begin{aligned} \dot{V}_v(v_i) \leq & \left(X_v(u_{d,i}, u_c) \left(\frac{2}{n} |\iota(\xi)| + \frac{3}{n \Delta(\mathbf{p}_b^p)} \right) + Y_v(u_{d,i}, u_c) \right) v_i^2 \\ & + \left(\frac{2}{n} |\iota(\xi)| + \frac{3}{n \Delta(\mathbf{p}_b^p)} \right) \left(\sum_{j \in \{1, \dots, n\} \setminus \{i\}} (|u_j| + |v_j| + |w_j|) + |u_i| + |w_i| \right) \\ & + (|H_v(\cdot)| - Y_v(u_{d,i}, u_c) |v_c|) |v_i|. \end{aligned} \quad (136)$$

For a sufficiently large v_i , the quadratic term will dominate the linear term. Therefore, we can conclude that v_i is bounded if

$$X_v(u_{d,i}, u_c) \left(\frac{2}{n} |\iota(\xi)| + \frac{3}{n \Delta(\mathbf{p}_b^p)} \right) + Y_v(u_{d,i}, u_c) < 0. \quad (137)$$

From the definition of the lookahead distance (40), this condition is satisfied if

$$\Delta_0 > \frac{3}{n \left| \frac{Y_v(u_{d,i}, u_c)}{X_v(u_{d,i}, u_c)} \right| - 2 |\iota(\xi)|}. \quad (138)$$

Now, we perform a similar procedure for the heave dynamics. We take the Lyapunov function candidate V_w from (105)

and simplify its derivative by setting $\tilde{\mathbf{X}}_2 = \mathbf{0}$.

$$\dot{V}_w(w_i) = X_w(u_{d,i}, u_c) q_{d,i} w_i + Y_w(u_{d,i}, u_c) (w_i - w_c) w_i + G(\theta_i) w_i. \quad (139)$$

Next, we find an upper bound on $q_{d,i} w_i$. We substitute from (94), set $\tilde{\mathbf{X}}_2 = \mathbf{0}$ and collect all terms that grow linearly with w_i to obtain the following expression

$$\begin{aligned} q_{d,i} w_i &= w_i \left(1 + \frac{\Delta(\mathbf{p}_b^p) x_b^p}{\Delta(\mathbf{p}_b^p)^2 + (x_b^p)^2} \right) \kappa(\xi) \frac{1}{n} \sum_{j=1}^n U_j \Omega_x(\gamma_j, \theta_p, \chi_j, \psi_p) - \frac{z_b^p w_i \sum_{j=1}^n \left(\frac{\cos(\gamma_{\text{LOS}}) y_b^p}{\sqrt{\Delta(\mathbf{p}_b^p)^2 + (y_b^p)^2}} + \frac{z_b^p}{\sqrt{\Delta(\mathbf{p}_b^p)^2 + (z_b^p)^2}} \right)}{n \Delta(\mathbf{p}_b^p) (\Delta(\mathbf{p}_b^p)^2 + (z_b^p)^2)} \\ &\quad + \frac{w_i \Delta(\mathbf{p}_b^p) \sum_{j=1}^n \frac{z_b^p}{\sqrt{\Delta(\mathbf{p}_b^p)^2 + (z_b^p)^2}}}{n (\Delta(\mathbf{p}_b^p)^2 + (z_b^p)^2)} + u_{d,i} \frac{Y_w(u_{d,i}, u_c)}{u_{d,i}^2 + w_i^2} w_i^2 + H_w(u_{d,i}, u_c, v_c, w_i, v_i, q_i, \mathbf{p}_b^p, \xi), \end{aligned} \quad (140)$$

$$\begin{aligned} H_w(\cdot) &= \left(\left(1 + \frac{\Delta(\mathbf{p}_b^p) x_b^p}{\Delta(\mathbf{p}_b^p)^2 + (x_b^p)^2} \right) k_\xi \kappa(\xi) \frac{x_b^p}{\sqrt{1 + (x_b^p)^2}} - \frac{y_b^p k_\xi x_b^p}{\sqrt{1 + (x_b^p)^2} \Delta(\mathbf{p}_b^p) (\Delta(\mathbf{p}_b^p)^2 + (y_b^p)^2)} \right. \\ &\quad \left. + u_{d,i} \frac{X_w(u_{d,i}, u_c) r_i - Y_w(u_{d,i}, u_c) v_c}{u_{d,i}^2 + w_i^2} \right) w_i. \end{aligned} \quad (141)$$

We can bound this expression as

$$|q_{d,i} w_i| \leq \left(\frac{2}{n} |\kappa(\xi)| + \frac{3}{n \Delta(\mathbf{p}_b^p)} \right) |w_i| \sum_{j=1}^n (|u_j| + |v_j| + |w_j|) + |H_w(\cdot)| \quad (142a)$$

$$\begin{aligned} &\leq \left(\frac{2}{n} |\kappa(\xi)| + \frac{3}{n \Delta(\mathbf{p}_b^p)} \right) w_i^2 + \left(\frac{2}{n} |\kappa(\xi)| + \frac{3}{n \Delta(\mathbf{p}_b^p)} \right) \left(\sum_{j \in \{1, \dots, n\} \setminus \{i\}} (|u_j| + |v_j| + |w_j|) + |u_i| + |w_i| \right) \\ &\quad + |H_w(\cdot)|, \end{aligned} \quad (142b)$$

which we can substitute to (139) to obtain

$$\begin{aligned} \dot{V}_w(w_i) &\leq \left(X_w(u_{d,i}, u_c) \left(\frac{2}{n} |\kappa(\xi)| + \frac{3}{n \Delta(\mathbf{p}_b^p)} \right) + Y_w(u_{d,i}, u_c) \right) w_i^2 \\ &\quad + \left(\frac{2}{n} |\kappa(\xi)| + \frac{3}{n \Delta(\mathbf{p}_b^p)} \right) \left(\sum_{j \in \{1, \dots, n\} \setminus \{i\}} (|u_j| + |v_j| + |w_j|) + |u_i| + |w_i| \right) \\ &\quad + (|H_w(\cdot)| - Y_w(u_{d,i}, u_c) |v_c|) |w_i|. \end{aligned} \quad (143)$$

For a sufficiently large w_i , the quadratic term will dominate the linear term. Therefore, we can conclude that w_i is bounded if

$$X_w(u_{d,i}, u_c) \left(\frac{2}{n} |\kappa(\xi)| + \frac{3}{n \Delta(\mathbf{p}_b^p)} \right) + Y_w(u_{d,i}, u_c) < 0. \quad (144)$$

From the definition of the lookahead distance (40), this condition is satisfied if

$$\Delta_0 > \frac{3}{n \left| \frac{Y_w(u_{d,i}, u_c)}{X_w(u_{d,i}, u_c)} \right| - 2 |\kappa(\xi)|}. \quad (145)$$